# Stability Analysis and Geometric Control for a Bluff-Body Hydrodynamic Vehicle

Sierra A. Adibi

A thesis
submitted in partial fulfillment of the
requirements for the degree of

Master of Science

University of Washington

2018

Committee:

Kristi A. Morgansen

Sam Burden

Program Authorized to Offer Degree:
Aeronautics & Astronautics

University of Washington

**Abstract**

Stability Analysis and Geometric Control for a Bluff-Body Hydrodynamic Vehicle

Sierra A. Adibi

Chair of the Supervisory Committee:
Professor Kristi A. Morgansen
William E. Boeing Department of Aeronautics & Astronautics

In this work, the bluff-body hydrodynamic robotic system, RoboRay, is introduced, and an early framework for modeling, stability, and control is developed. A model is proposed for the system, including a fluid dynamics models that includes hydrodynamic forces and added mass and inertia considerations. Nonlinear and linear stability analyses are then performed on the system, and sufficient conditions for nonlinear stability are provided. A geometric backstepping controller with trajectory tracking is then developed for the system. Simulations are performed of both the controlled and uncontrolled system in order to better understand its behavior. The simulations provide insight into potentially highly stable modes, and guidelines for future controller improvement.

# TABLE OF CONTENTS

# LIST OF FIGURES

# LIST OF TABLES

# ACKNOWLEDGMENTS

The author wishes to express her sincerest gratitude to her academic advisor, Professor Kristi Morgansen, without whom she would not have been able to come anywhere near completing this project on time.

The author also wishes to thank her husband, Logan Adibi-Yliniemi, for his endless support throughout the long process of graduate school.

# DEDICATION

To my incredibly patient and loving husband.

# Chapter 1

# INTRODUCTION

As technology continues to improve, many applications that once required large, heavy, difficult to use machines are being taken over by smaller, lighter options. One area where this is extremely apparent is robotic systems. Multiagent systems, comprised of a number of smaller, less expensive robots offer promise for the exploration and monitoring of harsh and dangerous environments.

## *1.1 Motivation*

The use of a network of small, simple robots, capable of collecting and transmitting data, has applications varying from space exploration to ocean monitoring. A net of vehicles designed to fall slowly and in a coordinated way could take data on changing ocean temperature and currents to determine the effects of climate change. Vehicles designed for atmospheric reentry could gather information on the potential habitability of other planets by humans. A network of sensors could be dropped from a jet flying over disputed territory, and maintain their formation for coordinated communication as they descend.

In this work, we describe current efforts for the bluff-body hydrodynamic robotic system known as RoboRay. RoboRay is the first iteration working towards a lightweight, flexible vehicle to be used for exploration and environmental monitoring with scaling opportunities for use in a variety of fluids. The flexible platform will allow for small, embedded actuators and easy to predict fluid dynamics properties.

### *1.2 Background*

RoboRay was inspired by the work on Sprite Satellites currently being performed at Cornell University[1][12][13]. The Sprites are small, satellite-on-a-chip vehicles being designed for data collection in the earth's atmosphere while surviving reentry. The latest iterations of the Sprite vehicles remain unactuated, making holding a formation during descent or landing in a specified area impossible. Our long-term goals for the RoboRay project include developing a framework for stability and control of lightweight vehicles, such as the Sprites.

The major challenges that we face in the continued development of RoboRay are numerous. The unique structure and actuation of the vehicle does not lend it self well to many of the modeling tools used for hydrodynamic vehicles, requiring that a framework for such a vehicle be designed. Most of the work in underwater vehicles work in one of three platforms: gliders[4][10], submarines[17], and large vessels[19][22]. Work on these vehicles is often performed under an assumption of neutral-buoyancy, meaning that the gravitational and buoyant forces acting on the vehicle effectively cancel out. Due to the intended application of the RoboRay project, this is not a well-reasoned long-term assumption to make.

Another common assumption for underwater and surface vessels is that an ellipsoidal approximation can be used in developing vehicle and fluid dynamics models[6]. Indeed, this common model serves many applications well, however due to the unique structure of the RoboRay craft, a flat plate assumption serves as a more appropriate model. The need to approximate the vehicle as a system of flat plates presents a number of challenges in itself, specifically in that there is little practically useful information available on aero and hydrodynamics for a flat plate at varying angles of attack. Assuming a connection between a system of flat plates complicates the issue further.

We seek to utilize a reasonable cross section of literature on the modeling, stability, and control of underwater vehicles in order to begin developing our own framework. A significant part of building said framework here relies on the work on fin-actuated robots in [15], the work on gliders in [10], and the development of sufficient stability bounds for bottom-heavy

water vehicles in [9].

The development of the basic RoboRay model, as well as the uncontrolled equations of motion, were based on the work performed in [10] in addition to some basics in robotic modeling [16]. The implementation of shape states for control inputs, as well as the use of accessibility for underactuated systems is derived from [15] and [14]. The nonlinear stability analysis and development of geometric bounds for stability follow the work in [9]. The flat-plate modeling techniques for added mass and inertia are based largely on the experimental analysis performed in [11].

### *1.3 Contributions*

The major contributions of this work are as follows:

1. The development of a baseline strategy for implementing fluid dynamics models into the modeling and simulation of vehicles approximated as flat plates

2. The determination of sufficient requirements for vehicle stability and testing of those requirements against simulation

3. The framework for geometric control of the RoboRay vehicle

### *1.4 Thesis Layout*

The rest of this paper is structured as follows. Chapter 2 provides information regarding the modeling of the robot, as well as how the surrounding fluid is represented. Chapter 3 details both the linear and nonlinear stability analyses performed. Chapter 4 provides the basis for the controller developed to guide the vehicle along a prescribed trajectory. Chapter 5 provides the results of the simulations of the study. Finally, Chapter 6 provides the reader with the conclusions of the study, as well as future work for the project.

# Chapter 2
# SYSTEM MODELING

In this chapter, we will cover the RoboRay system model. In Section 2.1, we will describe the basic set-up and components of the physical robotic system as well as how those components are modeled, and in Section 2.2 we will cover how we model the fluid dynamics of the surrounding fluid. Finally, Section 2.3 steps through the derivation of the equations of motion for the system using Lagrangian Dynamics.

## *2.1 Description of System*

At the time of writing, RoboRay is in the late stages of design, with all of the components chosen, and some manufacturing already complete. In this section, we will describe the proposed design, as well as the simplified models that have been developed for analysis.

### *2.1.1 Robotic System Design*

The proposed robotic system is comprised of six major components: the square center of the vehicle, the four vehicle "wings", and the water-tight dome which sits on top of the vehicle center and contains most of the robot's electrical components. The vehicle center and wings are made from a 1.6 [mm] thick acrylic custom cut to specifications, and the water-tight dome is a slightly-modified commercially available model, also made primarily of acrylic. A diagram of the main model components can be found in Fig. 2.1.

The wings are attached to the center of the vehicle using nylon hinges and are actuated with small, waterproof servomotors which are attached to the center base, outside of the water-tight dome. Between the dome and center base sits a printed circuit board, which supplies power and communication information to the servomotors from the electrical com-

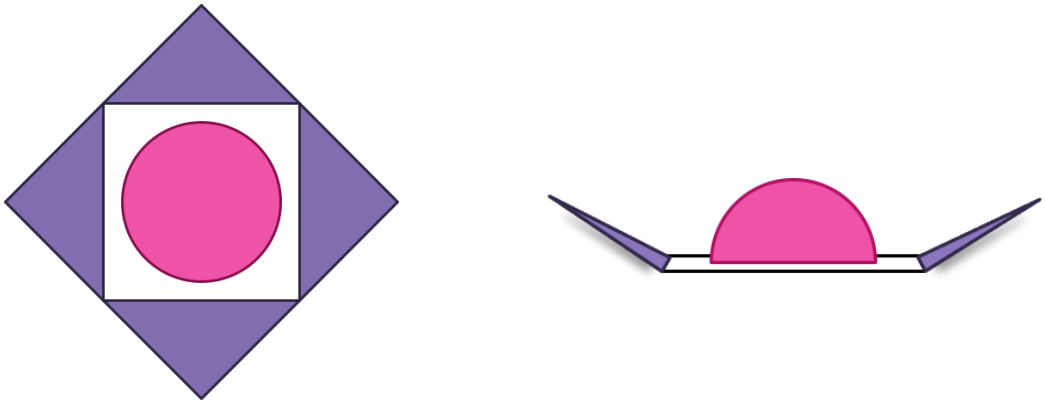

Top View Side View

Figure 2.1: Simplified diagrams of the RoboRay Vehicle. The pink circle represents the dome of the vehicle, the purple triangles represent the vehicle wings, and the white square is the acrylic center.

ponents inside the dome.

The majority of the system's power and processing components rest inside the water-tight dome. These components include the on-board processor, batteries, radio frequency module, and sensors.

### *2.1.2 Simplified Model*

The system model used for analysis in this work is comprised of the six main parts of the robot, without any consideration of the electronics and actuation on board. This allows the novel system to be studied using readily-available techniques. The wings and center base are modeled using flat-plate dynamics, and the dome is modeled as a hemisphere situated on top of the center. This model assumes that both the center of gravity (CG) and center of buoyancy (CB) for the vehicle are directly above the geometric center of the center base. As the wings deflect, the vertical position of both the CG and CB will change, however they will always remain aligned with the geometric center of the vehicle.

The vehicle has five on-board coordinate systems, one for each wing, as well as one

vehicle-fixed frame, which is originated at the CB. Each wing has a deflection angle, $s_i$, and the wing frame rotates along with $s_i$, so that the $x_i$ and $y_i$ axes always remain in-plane. For each wing, there is also a rotation matrix, $R_i$, which maps a vector from the wing-fixed frame to the vehicle-fixed frame. An illustration of the vehicle along with its reference frames can be found in Fig. 2.2.

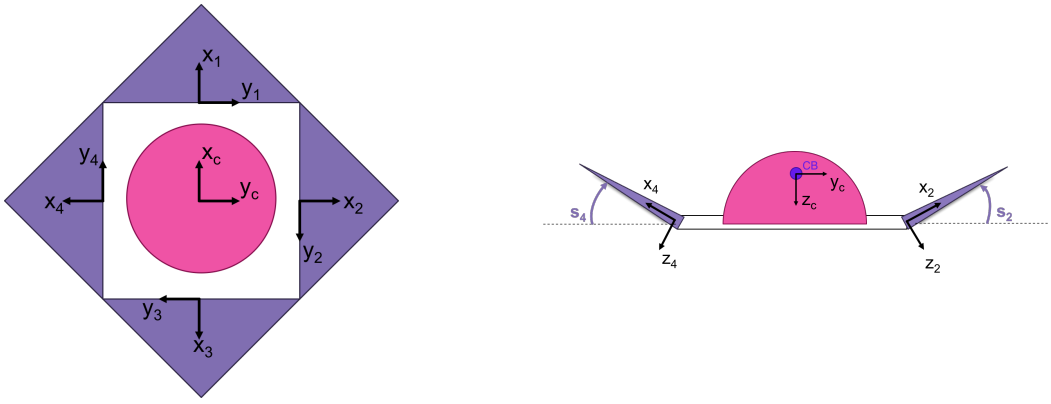


Top View Side View

Figure 2.2: Location of wing and vehicle-fixed coordinate frames for the RoboRay vehicle.

The $x_c$ and $y_c$ axes remain in-plane with the center acrylic square of the vehicle, while the $z_c$ axis points vertically in the direction of the vehicle's geometric center. The vector pointing from the CB to the CG is defined as $r_G = \ell z_c$, where in the case of the CG being higher than the CB, the direction of $z_c$ remains the same, and $\ell < 0$.

The position and orientation of the vehicle are described with respect to an inertial frame by the position vector, $\mathbf{b}$, which points from the origin of the inertial frame to the origin of the vehicle frame, and the rotation matrix, $R$, which maps a vector from the vehicle frame to the inertial frame. The velocity vectors, $V_c$ and $\Omega_c$, represent the translational and rotational vehicle velocities, respectively, in the vehicle-fixed frame. Figure 2.3 illustrates the position, orientation, and velocity states of the vehicle.

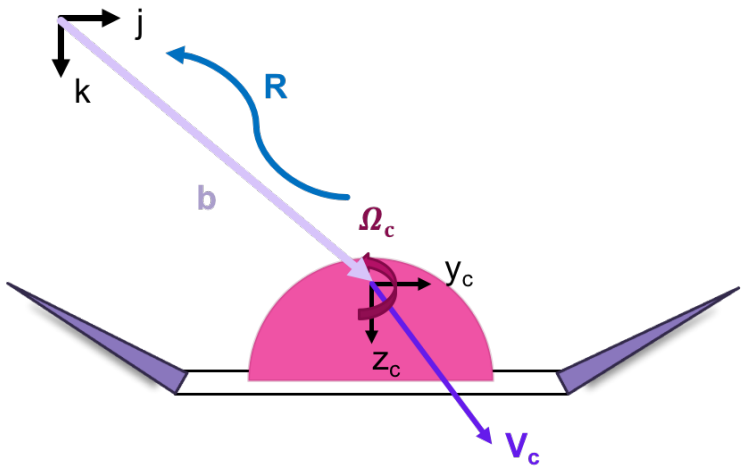


Figure 2.3: The states of interest include the position, orientation, and translational and rotational velocities of the vehicle.

## *2.2 Fluid Dynamics of System Model*

The fluid dynamics of the system are based on flat-plate aerodynamic studies available in literature [11]. The two main fluid dynamics concepts utilized in the model are hydrodynamic drag from pressure on the front of the plate and the added mass and inertia of accelerating the fluid surrounding the vehicle.

### *2.2.1 Drag Model*

Due to the unique physical geometry of the system, typical flat-plate lift and drag coefficients for varying angles of attack do not translate well. As the un-smooth geometry of the vehicle does not lend itself well to computational fluid dynamics techniques, it was determined that an analytical model should be used until experimental data could be gathered on the performance of the vehicle, and then integrated into the modeling and simulations.

The preliminary drag model chosen consists of two parts: translational drag acting perpendicular to each of the vehicle surfaces, and rotational drag acting perpendicular to the vehicle's center. The translational drag is calculated by mapping the free-stream air velocity,

$V_\infty$, into the local frame for a given surface. The velocity is then projected into the frame's $z$ axis, and the projection of the velocity is used to calculate the drag on that surface. Local drag is calculated using the following equation:

$$D_i = \frac{1}{2} C_D \rho A_i V_{\infty,i}^2$$

where $C_D = 1.28$ is the coefficient of drag for a flat plate perpendicular to fluid flow [2], $\rho$ is the density of the fluid, $A_i$ is the area of the surface, and $V_{\infty,i}$ is the projection of the freestream velocity into the local $z$ axis. Figure 2.4 illustrates how drag is calculated for each surface. As we are using a perpendicular, flat-plate assumption for the drag, the lift on the vehicle is assumed to be negligible.

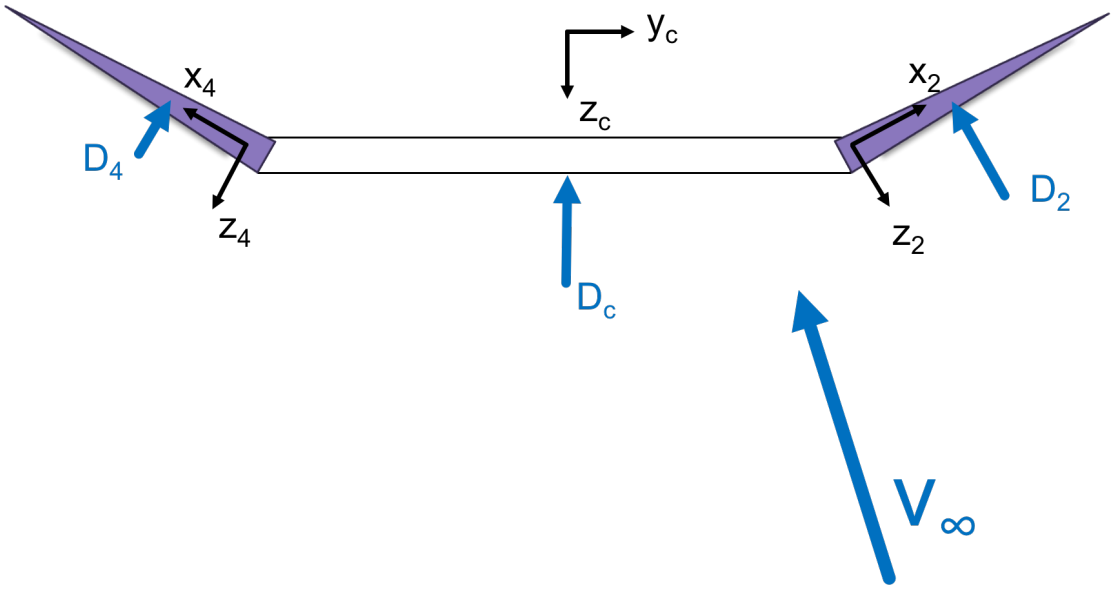


Figure 2.4: Drag on each surface of RoboRay as determined by the freestream air velocity.

The rotational drag is calculated by first approximating the vehicle as a circle with equal area. Using this approximation, a pseudo-radius is determined as:

$$r_p = \sqrt{A/\pi}.$$

The rotational drag is then integrated over the surface of the circle to determine a total rotational drag for a single direction:

$$M_{D_i} = \frac{1}{2} C_D \rho \int_0^{r_p} (2\pi r)(\omega_i r)^2 dr \tag{2.1}$$

where $\omega_i$ is the angular velocity of the vehicle around a given axis. Equation 2.1 holds for rotations about the $x_c$ and $y_c$ axes, however as the flat plate assumption has been made, there is no rotational drag about the $z_c$ axis.

### *2.2.2 Added Mass and Inertia*

Due to the low density of the vehicles as compared to the surrounding fluids, the acceleration of the fluids could not be reasonably ignored in the development of the system dynamics. Added mass and inertia approximations were determined for each component, translated into a central body coordinate frame, and summed to determine the approximation for the system. Each component was approximated as a flat-plate wing, and the added mass calculations were performed according to [11]. The added mass for the hemisphere is considered to be negligible in comparison to the effects of the center and wing flat plates.

The translational added mass for each component was considered only in the local $z_i$ direction, in order to maintain consistency with the flat plate assumption. The translational added mass was calculated according to:

$$m_{i_z}^f = \frac{\pi}{4} \rho k \bar{c}^2 b \tag{2.2}$$

where $k$, the coefficient of added mass, is determined from the aspect ratio, $\bar{c}$ is the average chord of the wing, and $b$ is the wing span. Table 2.1 contains the coefficients used for each component.

The added inertia for each component was considered about the local $x_i$ and $y_i$ axis. The equations for the added inertia for an individual control surface about its $x_i$ and $y_i$ axis (respectively) are:

Table 2.1: Added mass and inertia coefficients for vehicle center and wings [11].

| **System Component** | $k$ | $D_\lambda$ | $k'_x$ | $k'_y$ |
|---|---|---|---|---|
| Vehicle Center | $\sqrt{2}/2$ | 1 | 0.41 | 0.41 |
| Control Surface | 0.91 | 0.6 | 0.75 | 0.15 |

$$J^f_{i_x} = \frac{\pi}{48}\rho D_\lambda k'_x \bar{c}^2 b^3 \tag{2.3}$$

$$J^f_{f_y} = \frac{\pi}{48}\rho D_\lambda k'_y \bar{c}^3 b^2 + m^f_{i_z} l^2 \tag{2.4}$$

where $D_\lambda, k'_x$ and $k'_y$ are correction factors determined from the taper and aspect ratio of the control surfaces modeled as wings and $l$ is the perpendicular distance from the centroid of the surface to the leading edge.

### *2.3 Derivation of the Equations of Motion*

The system's equations of motion were developed using Lagrangian Mechanics in order to ensure the complicated system was modeled as accurately as possible. In order to limit the number of total states to track, first the translational and rotational velocities of each wing, $V_i$ and $\Omega_i$, respectively, were expressed in terms of the velocities of the vehicle center:

$$V_i = V_c - \hat{r}_{LE_i}\Omega_c - R_i \hat{r}_{CG_i}\dot{S}_i \tag{2.5}$$

$$\Omega_i = \Omega_c + R_i \dot{S}_i \tag{2.6}$$

where $r_{LE_i}$ is the vector from the origin of the vehicle-fixed frame to the origin of the local wing frame, $r_{CG_i}$ is the vector from the origin of the local wing frame to the centroid of the wing, and $\dot{S}_i$ is the rate of angular deflection of the wing with respect to the vehicle center. The $\hat{\cdot}$ donation on a vector represents its transformation into a skew-symmetric matrix, where

right-multiplying the matrix by a vector is equivalent to taking the cross product of the two vectors. The matrix is formed as:

$$\hat{r} = \begin{bmatrix} 0 & -r_3 & r_2 \\ r_3 & 0 & -r_1 \\ -r_2 & r_1 & 0 \end{bmatrix}.$$

With all of the velocities expressed in terms of the vehicle center velocities, it was then possible to express the kinetic energy of the system using the states $V_c, \Omega_c$, and the vector of angular deflections of the wings, $\dot{S} = [\dot{S}_1^T, \dot{S}_2^T, \dot{S}_3^T, \dot{S}_4^T]^T$. The potential energy of the system has two components: there are the translational effects of gravity and buoyancy, as well as the moment that occurs as a result of the non-coincident centers of buoyancy and gravity. By taking the difference between the kinetic and potential energies of the system, we developed the system Lagrangian:

$$L = \frac{1}{2}\left(V_c^T \tilde{M} V_c + \Omega_c^T \tilde{J} \Omega_c + 2\Omega_c^T \tilde{D} V_c\right) - m_v a_w (d_{max} - \mathbf{b}\cdot\mathbf{k}) + m_v a_w \ell \left(R^T \mathbf{k} \cdot z_c\right). \quad (2.7)$$

In Eq. 2.7, $m_v$ is the total mass of the vehicle, $a_w$ is the acceleration experienced by the vehicle when considering both gravity and buoyancy, and $d_{max}$ is the maximum reachable depth of the vehicle. The $\tilde{M}$, $\tilde{J}$, and $\tilde{D}$ matrices are the mass, inertia, and cross term matrices for the entire vehicle. Each of these matrices were determined by performing an expansion of the kinetic energy of each vehicle component, and collecting terms for simplicity. They are defined as:

$$\tilde{M} = M_c + \sum_{i=1}^{4} M_i$$

$$\tilde{D} = D_c + \sum_{i=1}^{4} \hat{r}_{LE_i} M_i$$

$$\tilde{J} = J_c + \sum_{i=1}^{4} J_i - \hat{r}_{LE_i} M_i \hat{r}_{LE_i}$$

where $M_i = R_i M_{w_i} R_i^T$ and $J_i = R_i J_{w_i} R_i^T$ are the mass and inertia matrices of the $i$th wing expressed in the vehicle-fixed frames. Correspondingly, $M_{w_i}$ and $J_{w_i}$ are the mass and inertia matrices expressed in the local wing frame. A full description of the process to compute these matrices can be found in Appendix A.

Lagrange's Equations were then used to determine the equations of motion for the velocity states:

$$\frac{d}{dt}\left(\frac{\partial L}{\partial \dot{q}_i}\right) = \frac{\partial L}{\partial q_i} + \Upsilon_{ext_i}$$

where $q_i$ is a system state and $\Upsilon_{ext_i}$ is the net external force acting on that system state [16]. The derivatives of the position, orientation, and wing deflection states were found using relative motion, and the equations of motion for the system were found as:

$$\frac{d}{dt}\begin{bmatrix} \mathbf{b} \\ R \\ S \end{bmatrix} = \begin{bmatrix} RV_c \\ R\hat{\Omega}_c \\ \dot{S} \end{bmatrix}$$

$$\begin{aligned} \dot{V}_c &= m_v a_w C\mathbf{k} - m_v a_w \ell B(R^T\mathbf{k} \times z_c) + CF_{ext} + BM_{ext} - \left(C\dot{\tilde{M}} + B\dot{\tilde{D}}\right)V_c \\ &\quad - \left(C\dot{\tilde{D}}^T + B\dot{\tilde{J}}\right)\Omega_c - \left(C\dot{\mathcal{A}}_1^T + B\dot{\mathcal{A}}_2^T\right)\dot{S} - \left(C\mathcal{A}_1^T + B\mathcal{A}_2^T\right)\ddot{S} \end{aligned} \tag{2.8}$$

$$\begin{aligned} \dot{\Omega}_c &= m_v a_w B^T\mathbf{k} - m_v a_w \ell A(R^T\mathbf{k} \times z_c) + B^T F_{ext} + AM_{ext} - \left(B^T\dot{\tilde{M}} + A\dot{\tilde{D}}\right)V_c \\ &\quad - \left(B^T\dot{\tilde{D}}^T + A\dot{\tilde{J}}\right)\Omega_c - \left(B^T\dot{\mathcal{A}}_1^T + A\dot{\mathcal{A}}_2^T\right)\dot{S} - \left(B^T\mathcal{A}_1^T + A\mathcal{A}_2^T\right)\ddot{S} \end{aligned} \tag{2.9}$$

$$\ddot{S} = u \tag{2.10}$$

where the new matrices above are defined as:

$$A = \left(\tilde{J} - \tilde{D}\tilde{M}^{-1}\tilde{D}^T\right)^{-1} \qquad B = -M^{-1}\tilde{D}^T A = -CD^T J^{-1}$$

$$C = \left(\tilde{M} - \tilde{D}^T\tilde{J}^{-1}\tilde{D}\right)^{-1}$$

$$\mathcal{A}_1 = \begin{bmatrix} \hat{r}_{CG_1} M_{w_1} R_1^T \\ \hat{r}_{CG_2} M_{w_2} R_2^T \\ \hat{r}_{CG_3} M_{w_3} R_3^T \\ \hat{r}_{CG_4} M_{w_4} R_4^T \end{bmatrix} \qquad \mathcal{A}_2 = \begin{bmatrix} -\hat{r}_{CG_1} M_{w_1} R_1^T \hat{r}_{LE_1} \\ -\hat{r}_{CG_2} M_{w_2} R_2^T \hat{r}_{LE_2} \\ -\hat{r}_{CG_1} M_{w_3} R_3^T \hat{r}_{LE_3} \\ -\hat{r}_{CG_4} M_{w_4} R_4^T \hat{r}_{LE_4} \end{bmatrix}$$

Further details on the derivation of the equations of motion can be found in Appendix A.

# Chapter 3

# STABILITY ANALYSIS

In this chapter, we examine the stability of the vehicle-fluid system from two perspectives. First, following the work in [9], we take a nonlinear approach by studying the system Hamiltonian and finding geometric bounds for the system stability of two different equilibria for the modified, unforced system. Then, we use those same equilibria to linearize the system about, and perform a spectral stability analysis of the full system model.

## *3.1 Nonlinear Analysis*

In this section, we examine the unforced, neutrally buoyant system, which allows us to follow the stability analysis performed in [9]. While this is inherently an incomplete model, it does allow for the examination of the nonlinear system, as well as the development of some interesting potential equilibria.

### *3.1.1 Unforced System Dynamics*

In order to model the unforced system dynamics, the system Lagrangian is first developed. As the wings are unactuated, they will have the same rotational velocity as the center of the system, and the velocity of each with can be determined using relative motion. Expressing the energy of each wing in terms of the rotational and translational velocities of the center provides for the convenient definition of four new matrices,

$$\breve{M} = M_c + \sum_{i=1}^{4} M_i$$
$$\breve{D} = D_c + \sum_{i=1}^{4} \hat{r}^c_{CG_i} M_i$$
$$\breve{J} = J_c + \sum_{i=1}^{4} J_i - \hat{r}^c_{CG_i} M_i R^c_{CG_i}$$

where $\hat{r}^c_{CG_i}$ is the vector from the CG of the vehicle to the CG of the $i$th wing, expressed in the center vehicle frame. The matrices above can be used to form the slightly modified version of the neutrally-buoyant system Lagrangian:

$$L = \frac{1}{2}\left(V_c^T \breve{M} V_c + 2\Omega_c^T \breve{D} V_c + \Omega_c^T \breve{J} \Omega_c\right) + m_v a_w l \left(\mathbf{k} \cdot R\mathbf{z}_c\right). \tag{3.1}$$

The applicability of the above Lagrangian to the work in [9] depends largely on the modified matrices taking on convenient shapes. Specifically, $\breve{M}$ and $\breve{J}$ must be diagonal matrices, and $\breve{D}$ must take the following form:

$$\breve{D} = \begin{bmatrix} 0 & -d_1 & 0 \\ d_2 & 0 & 0 \\ 0 & 0 & 0 \end{bmatrix}$$

The necessary shapes for applicability occur when the angular deflections of opposite wings are equal to each other; $s_1 = s_3, s_2 = s_4$. This then ensures that the symmetry groups from [9] hold, and that we can utilize the same Hamiltonian and Casimir functions, with matrix definitions based on our system dynamics:

$$\Pi = \breve{J}\Omega_c + \breve{D} V_c \qquad P = \breve{M} V_c + \breve{D}^T \Omega_c$$
$$\Gamma = R^T \mathbf{k} \qquad \breve{A} = (\breve{J} - \breve{D}\breve{M}^{-1}\breve{D}^T)^{-1}$$
$$\breve{B} = -\breve{C}\breve{D}^T\breve{J}^{-1} = -\breve{M}^{-1}\breve{D}^T\breve{A} \qquad \breve{C} = (\breve{M} - \breve{D}^T\breve{J}^{-1}\breve{D})^{-1}.$$

From the above, we can see that our new matrices will take the following forms:

$$\breve{A} = \begin{bmatrix} \frac{m_2}{I_1 m_2 - d_1^2} & 0 & 0 \\ 0 & \frac{m_1}{I_2 m_1 - d_2^2} & 0 \\ 0 & 0 & \frac{1}{I_3} \end{bmatrix} \qquad \breve{B} = \begin{bmatrix} 0 & \frac{-d_2}{I_2 m_1 - d_2^2} & 0 \\ \frac{d_1}{I_1 m_2 - d_1^2} & 0 & 0 \\ 0 & 0 & 0 \end{bmatrix}$$

$$\breve{C} = \begin{bmatrix} \frac{I_2}{I_2 m_1 - d_2^2} & 0 & 0 \\ 0 & \frac{I_1}{I_1 m_2 - d_1^2} & 0 \\ 0 & 0 & \frac{1}{m_3} \end{bmatrix}$$

The ability to utilize matrices of similar shape as those in [9] allows us to with similar assumptions. Thus, we will study two particular equilibria of interest, one with and one without spin. The stability analysis of each of these equilibria are provided in the following sections.

### *3.1.2 Stability Analysis of Equilibrium Without Spin*

The equilibrium point of the system without spin which will be explored in this section includes velocity in two directions, one vertical and one horizontal. This equilibrium takes the following form:

$$\Omega_{e1} = \begin{bmatrix} 0 \\ 0 \\ 0 \end{bmatrix} \quad V_{e1} = \begin{bmatrix} 0 \\ v_{e1_2} \\ v_{e1_3} \end{bmatrix} \quad \Gamma_{e1} = \begin{bmatrix} 0 \\ \frac{(m_2 - m_3) v_{e1_2} v_{e1_3}}{m_v a_w \ell} \\ \sqrt{1 - \left( \frac{(m_2 - m_3) v_{e1_2} v_{e1_3}}{m_v a_w \ell} \right)^2} \end{bmatrix}. \tag{3.2}$$

In order to determine where the equilibrium was Lyapunov stable, the Jacobian and Hessian of the Hamiltonian, $H_\Phi$ were studied:

$$H = \frac{1}{2} \left( \Pi^T \breve{A} \Pi + 2 \Pi^T \breve{B}^T P + P^T \breve{C} P \right) - m_v a_w \ell (\Gamma \cdot z_c)$$

$$H_\Phi = H + \Phi(P \cdot \Gamma, \|P\|^2, \|\Gamma\|^2)$$

First, the Jacobian of the system was found and set to zero in order to determine the critical point:

$$\nabla H + \nabla \Phi = 0$$

$$\begin{bmatrix} 0 \\ 0 \\ 0 \\ 0 \\ v_{e1_2} \\ v_{e1_3} \\ 0 \\ 0 \\ -m_v a_w \ell \end{bmatrix} + \begin{bmatrix} 0 \\ 0 \\ 0 \\ 0 \\ \dot{\Phi}\frac{(m_2-m_3)v_{e1_2}v_{e1_3}}{m_v a_w \ell} + 2\Phi' m_2 v_{e1_2} \\ \dot{\Phi}\sqrt{1-\left(\frac{(m_2-m_3)v_{e1_2}v_{e1_3}}{m_v a_w \ell}\right)^2} + 2\Phi' m_3 v_{e1_3} \\ 0 \\ \dot{\Phi} m_2 v_{e1_2} + 2\Phi^\dagger \frac{(m_2-m_3)v_{e1_2}v_{e1_3}}{m_v a_w \ell} \\ \dot{\Phi} m_3 v_{e1_3} + 2\Phi^\dagger \sqrt{1-\left(\frac{(m_2-m_3)v_{e1_2}v_{e1_3}}{m_v a_w \ell}\right)^2} \end{bmatrix} = 0$$

where in the above:

$$\dot{\Phi} = \frac{\partial \Phi}{\partial P \cdot \Gamma} \qquad \Phi' = \frac{\partial \Phi}{\partial \|P\|^2} \qquad \Phi^\dagger = \frac{\partial \Phi}{\partial \|\Gamma\|^2}$$

all evaluated at the equilibria.

Operating under the assumption that $\dot{\Phi} = 0$, it is then necessary to make one of two assumptions; that $m_2 - m_3 = 0$ or that $v_{e1_2} = 0$. In order to simplify the geometric constraints, it was decided to neglect the translational velocity term. This simplified the remaining unknown terms to:

$$2\Phi' = -1/(m_3)$$

$$2\Phi^\dagger = m_v a_w \ell$$

The system Hessian was then found as

$$\nabla^2 H + \nabla^2 \Phi$$

$$= \begin{bmatrix} a_1 & 0 & 0 & 0 & b_2 & 0 & 0 & 0 & 0 \\ 0 & a_2 & 0 & b_1 & 0 & 0 & 0 & 0 & 0 \\ 0 & 0 & a_3 & 0 & 0 & 0 & 0 & 0 & 0 \\ 0 & b_1 & 0 & c_1 - \frac{1}{m_3} & 0 & 0 & 0 & 0 & 0 \\ b_2 & 0 & 0 & 0 & c_2 - \frac{1}{m_3} & 0 & 0 & 0 & 0 \\ 0 & 0 & 0 & 0 & 0 & a + cm_3^2 v_{e1_3}^2 & 0 & 0 & am_3 v_{e1_3} \\ 0 & 0 & 0 & 0 & 0 & 0 & m_v a_w \ell & 0 & 0 \\ 0 & 0 & 0 & 0 & 0 & 0 & 0 & m_v a_w \ell & 0 \\ 0 & 0 & 0 & 0 & 0 & am_3 v_{e1_3} & 0 & 0 & m_v a_w \ell + am_3^2 v_{e1_3}^2 \end{bmatrix}$$

where

$$a = \ddot{\Phi} \qquad\qquad c = 4\Phi''.$$

In order for the system to be stable, it was necessary for the Hessian to be positive definite. To find sufficient conditions for positive definiteness, an $LDL^T$ decomposition was performed, and the values of the diagonal matrix were assumed to be positive:

$$D_1 = a_1 \qquad D_2 = a_2 \qquad D_3 = a_3$$

$$D_4 = \frac{1}{m_1} - \frac{1}{m_3} \qquad D_5 = \frac{1}{m_2} - \frac{1}{m_3} \qquad D_6 = a + cm_3^2 v_{e1_3}^2$$

$$D_7 = m_v a_w \ell \qquad D_8 = m_v a_w \ell \qquad D_9 = m_v a_w \ell + \frac{acm_3^4 v_{e1_3}^4}{a + cm_3^2 v_{e1_3}^2}$$

More information on this process can be found in Appendix B.

It was found that for stability to be guaranteed, there were three sufficient conditions:

$$\ell > 0 \qquad\qquad m_3 > m_1 \qquad\qquad m_3 > m_2$$

### *3.1.3 Stability Analysis of Equilibrium With Spin*

The equilibrium point of the system with spin, which will be explored in this section, assumes that the vehicle is moving straight down in the direction of gravity, and rotating about the gravitational axis. This equilibrium takes the following form:

$$\Omega_{e2} = \begin{bmatrix} 0 \\ 0 \\ \omega_{e2_3} \end{bmatrix} \quad V_{e2} = \begin{bmatrix} 0 \\ 0 \\ v_{e2_3} \end{bmatrix} \quad \Gamma_{e2} = \begin{bmatrix} 0 \\ 0 \\ 1 \end{bmatrix}. \tag{3.3}$$

The process of determining the stability for this equilibrium followed that described in the previous section. It was found that for stability to be guaranteed, there were three sufficient conditions:

$$\ell > 0 \qquad m_3 > m_1 \qquad m_3 > m_2$$

The above conditions match the conditions required for the equilibrium without spin, suggesting that for this simplified model these are reliable criteria.

## *3.2 Linear Analysis*

In order to further evaluate the equilibria developed using Leonard's technique in [9], the system was linearized and a spectral stability analysis was performed by determining the eigenvalues of the state matrix. A variety of possible values for the equilibria were chosen and tested, in order to determine if there were any patterns in the results.

### *3.2.1 Spectral Stability Analysis of Equilibria Without Spin*

In the case of the equilibria without spin, the only configurations found to be stable necessitated that the wings be either fully flat or folded up to 90°. Table 3.1 details all of the configurations found to be stable without spin by the spectral analysis.

Table 3.1: Vehicle Configurations which met spectrally stable requirements for the no spin equilibrium.

| $\ell$ [m] | $s_1$ [°] | $s_2$ [°] | $v_2$ [m/s] | $v_3$ [m/s] | $m_1$ [kg] | $m_2$ [kg] | $m_3$ [kg] |
|---|---|---|---|---|---|---|---|
| 0.0167 | 0 | 0 | 0 | 1 | 1.0625 | 1.0625 | 2.2645 |
| 0.0167 | 0 | 0 | 0 | 2 | 1.0625 | 1.0625 | 2.2645 |
| 0.0167 | 0 | 0 | 1 | 1 | 1.0625 | 1.0625 | 2.2645 |
| 0.0167 | 0 | 0 | 1 | 2 | 1.0625 | 1.0625 | 2.2645 |
| 0.0171 | 0 | 90 | 1 | 1 | 1.0625 | 1.6069 | 1.7201 |
| 0.0171 | 0 | 90 | 1 | 2 | 1.0625 | 1.6069 | 1.7201 |

### *3.2.2 Spectral Stability Analysis of Equilibria With Spin*

In the case of the equilibria with spin, the only configurations found to be stable were those in which there was no wing deflection. Table 3.2 details all of the configurations found to be stable with spin by the spectral analysis.

Upon further investigation into the eigenvalues associated with the vehicle configurations, it was found that for a number of configurations with angular deflections between the extremes of flat 0° and 90°, the maximum real part of the eigenvalues were less than 1. While these configurations can not be considered spectrally stable, they do suggest that some other configurations may be interesting to explore in simulation.

Table 3.2: Vehicle Configurations which met spectrally stable requirements for the equilibrium with spin.

| $\ell$ [m] | $s_1$ [°] | $s_2$ [°] | $v_3$ [m/s] | $\omega_3$ [m/s] | $m_1$ [kg] | $m_2$ [kg] | $m_3$ [kg] |
|---|---|---|---|---|---|---|---|
| 0.0167 | 0 | 0 | 0.3 | 0.1 | 1.0625 | 1.0625 | 2.2645 |
| 0.0167 | 0 | 0 | 0.3 | 0.5 | 1.0625 | 1.0625 | 2.2645 |
| 0.0167 | 0 | 0 | 0.3 | 1 | 1.0625 | 1.0625 | 2.2645 |
| 0.0167 | 0 | 0 | 0.5 | 0.1 | 1.0625 | 1.0625 | 2.2645 |
| 0.0167 | 0 | 0 | 0.5 | 0.5 | 1.0625 | 1.0625 | 2.2645 |
| 0.0167 | 0 | 0 | 0.5 | 1 | 1.0625 | 1.0625 | 2.2645 |
| 0.0167 | 0 | 0 | 1 | 0.1 | 1.0625 | 1.0625 | 2.2645 |
| 0.0167 | 0 | 0 | 1 | 0.5 | 1.0625 | 1.0625 | 2.2645 |
| 0.0167 | 0 | 0 | 1 | 1 | 1.0625 | 1.0625 | 2.2645 |

# Chapter 4

# SYSTEM CONTROL

In this chapter, we develop the controller for the system. To do so, we first assess the controllability of the system. We then lay the groundwork for the development of a backstepping controller, as well as the implementation of tracking a specified trajectory using that controller. Finally, we discuss the application of the controller to our system.

## *4.1 Controllability*

Before developing a controller for the system, it was first necessary to determine if the system was fully controllable. Doing so via nonlinear methods involves getting the system dynamics into a control affine form, then performing Lie Brackets between the drift vector field and the control vector fields. The resulting vector fields are then concatenated in order to determine the system Ideal. For a system Ideal with rank equal to the number of states of the system, we can determine the system is Short Term Locally Controllable (STLC) [14].

As the shape states are directly controlled in their second derivative, we are able to make some quick determinations of the controllability of those states. Examining only the shape states in control affine form:

$$\frac{d}{dt}\begin{bmatrix} S \\ \dot{S} \end{bmatrix} = \begin{bmatrix} \dot{S} \\ 0 \end{bmatrix} + \begin{bmatrix} 0 \\ 1 \end{bmatrix} u \tag{4.1}$$

Performing a Lie Bracket between the two vector fields above:

$$[f_0(S), f_1(S)] = \begin{bmatrix} 0 & 1 \\ 0 & 0 \end{bmatrix} \begin{bmatrix} 0 \\ 1 \end{bmatrix} - \begin{bmatrix} 0 & 0 \\ 0 & 0 \end{bmatrix} \begin{bmatrix} \dot{S} \\ 0 \end{bmatrix}$$
$$= \begin{bmatrix} 1 \\ 0 \end{bmatrix}$$

In order to determine the system Ideal, we can then horizontally concatenate the above vector field with the control vector field. Taking the rank of this new matrix:

$$\text{rank} \left( \begin{bmatrix} 0 & 1 \\ 1 & 0 \end{bmatrix} \right) = 2.$$

We see that the Ideal of the shape states is full rank, and that the shape states are STLC everywhere.

The controllability guarantee of the shape states allows us to examine a modified version of the equations of motion for controllability of the rest of the system. Examining the remaining states in control affine form:

$$\frac{d}{dt} \begin{bmatrix} \mathbf{b} \\ R \\ V \\ \Omega \end{bmatrix} = \begin{bmatrix} RV \\ R\hat{\Omega} \\ g_0(R, S, V, \Omega, \dot{S}) \\ h_0(R, S, V, \Omega, \dot{S}) \end{bmatrix} + \sum_{i=1}^{4} \begin{bmatrix} 0 \\ 0 \\ g_i(S) \\ h_i(S) \end{bmatrix} u_i$$

we take a representative Lie Bracket of the drift term with the $f_i$ vector field:

$$[f_0, f_i] = \begin{bmatrix} 0 & V & R^{\wedge} & 0 \\ 0 & \hat{\Omega} & 0 & R \\ 0 & \frac{\partial}{\partial R} g_0 & \frac{\partial}{\partial V} g_0 & \frac{\partial}{\partial \Omega} g_0 \\ 0 & \frac{\partial}{\partial R} h_0 & \frac{\partial}{\partial V} h_0 & \frac{\partial}{\partial \Omega} h_0 \end{bmatrix} \begin{bmatrix} 0 \\ 0 \\ g_i(S) \\ h_i(S) \end{bmatrix} - \begin{bmatrix} 0 & 0 & 0 & 0 \\ 0 & 0 & 0 & 0 \\ 0 & 0 & 0 & 0 \\ 0 & 0 & 0 & 0 \end{bmatrix} \begin{bmatrix} RV \\ R\hat{\Omega} \\ g_0(R, S, V, \Omega, \dot{S}) \\ h_0(R, S, V, \Omega, \dot{S}) \end{bmatrix}$$

$$= \begin{bmatrix} R^{\wedge} g_i(S) \\ R h_i(S) \\ \frac{\partial}{\partial V}(g_0) g_i(S) + \frac{\partial}{\partial \Omega}(g_0) h_i(S) \\ \frac{\partial}{\partial V}(h_0) g_i(S) + \frac{\partial}{\partial \Omega}(h_0) h_i(S) \end{bmatrix}$$

Examination of the above result reveals that as successive Lie Brackets are taken, it will be possible to obtain a full rank matrix for the system Ideal, thus ensuring that our system will be STLC.

### *4.2 Backstepping Controller Development*

In order to handle the system nonlinearities, a backstepping controller was chosen. In this section, we will provide some information on the general structure of the backstepping controller.Further information on backstepping controllers can be found in [5].

The backstepping controller depends on being able to transform the system dynamics into a system of equations with the following form:

$$\begin{aligned} \dot{\eta} &= F_a(\eta) + G_a(\eta)\xi \\ \dot{\xi} &= F_b(\eta, \xi) + G_b(\eta, \xi)u \end{aligned} \tag{4.2}$$

where $\dot{\eta}$ takes in $\xi$ as an input and $\dot{\xi}$ accepts the control input, $u$, directly. It is then assumed that there exists a positive definite function, $W(\eta)$, and a smooth, positive definite Lyapunov function, $V_a(\eta)$, such that:

$$\frac{\partial V_a}{\partial \eta} \left[ F_a(\eta) + G_a(\eta)\phi(\eta) \right] \leq -W(\eta)$$

where $\xi = \phi(\eta)$ is a state feedback control which stabilizes $\dot{\eta}$. By defining the state, $z = \xi - \phi(\eta)$, we can transform the system in Eq. 4.2, to take the form:

$$\begin{aligned} \dot{\eta} &= F_a(\eta) + G_a(\eta)\left(\phi(\eta) + z\right) \\ \dot{z} &= F_b(\eta, \xi) - \tfrac{\partial \phi}{\partial \eta}\dot{\eta} + G_b(\eta, \xi)u. \end{aligned} \tag{4.3}$$

We then define a new Lyapunov function for the system, utilizing the state variable, $z$:

$$V(\eta, \xi) = V_a(\eta) + \frac{1}{2} z^T z.$$

The derivative of the above Lyapunov function takes the form:

$$\dot{V} = \tfrac{\partial V_a}{\partial \eta}[F_a(\eta) + G_a(\eta)\phi(\eta)] + \tfrac{\partial V_a}{\partial \eta} G_a(\eta) z + z^T \dot{z} \tag{4.4}$$

where we know the first term to be negative definite. We can then choose our $u$ such that it will make the remaining terms negative definite, thus providing asymptotic stability of our system at the origin. Setting the second two terms above less than zero, we can solve for such a $u$:

$$\begin{aligned} \frac{\partial V_a}{\partial \eta} G_a(\eta) z + z^T \dot{z} &\leq 0 \\ z^T G_a(\eta)^T \frac{\partial V_a}{\partial \eta}^T + z^T \left( F_b(\eta, \xi) - \frac{\partial \phi}{\partial \eta}\dot{\eta} + G_b(\eta, \xi)u \right) &\leq 0 \\ G_a(\eta)^T \frac{\partial V_a}{\partial \eta}^T + F_b(\eta, \xi) - \frac{\partial \phi}{\partial \eta}\left(F_a(\eta) + G_a(\eta)\left(\phi(\eta) + z\right)\right) &\leq -G_b(\eta, \xi)u \\ -G_b^{\dagger}\left( G_a(\eta)^T \frac{\partial V_a}{\partial \eta}^T + F_b(\eta, \xi) - \frac{\partial \phi}{\partial \eta}\left(F_a(\eta) + G_a(\eta)\left(\phi(\eta) + z\right)\right) \right) &\geq u \end{aligned}$$

$$u = -G_b^{\dagger}\left( G_a(\eta)^T \frac{\partial V_a}{\partial \eta}^T + F_b(\eta, \xi) - \frac{\partial \phi}{\partial \eta}\left(F_a(\eta) + G_a(\eta)\left(\phi(\eta) + z\right)\right) + Kz \right) \tag{4.5}$$

In order for Eq. 4.4 to maintain negative definiteness, we choose $K$ to be a positive definite matrix. If we choose $\phi(0) = 0$, the origin of our system is asymptotically stable.

### *4.3 Trajectory Tracking with Backstepping*

In order to track a trajectory using backstepping, we first define the reference trajectory in terms of our backstepping states, $\eta_r, \dot{\eta}_r$ and $\dot{\xi}_r$. We can then define the error between our current states and reference trajectories as:

$$\delta_\eta = \eta - \eta_r \qquad\qquad \dot{\delta}_\eta = \dot{\eta} - \dot{\eta}_r$$

As $\xi$ is the input for the $\dot{\eta}$ function, we define our idealized function, $\xi_r = \phi$ to ensure stability in $\delta_\eta$:

$$\phi = \dot{\eta}_r - \delta_\eta$$
$$\xi = \delta_\xi + \phi$$

We can examine a candidate Lyapunov function which we will want to stabilize, as well as its derivative:

$$V = \frac{1}{2}\left(\delta_\eta^T \delta_\eta + \delta_\xi^T \delta_\xi\right)$$
$$\dot{V} = \delta_\eta^T \dot{\delta}_\eta + \delta_\xi^T \dot{\delta}_\xi$$

If we approximate $\dot{\eta}$ as $\xi$, we can redefine $\dot{\delta}_\eta$ in terms of our $\phi$:

$$\begin{aligned}\dot{\delta}_\eta &= -\dot{\eta}_r + \dot{\eta} \\ &= -\dot{\eta}_r + \delta_\xi + \phi \\ &= \delta_\xi - \delta_\eta\end{aligned}$$

We can then plug this form into our Lyapunov function derivative:

$$\dot{V} = -\delta_\eta^T \delta_\eta + \delta_\xi^T \left( \delta_\eta + \dot{\delta}_\xi \right)$$

The first term above will be negative definite by nature, so it is then necessary to define the second term as negative definite. We do so by defining some positive definite $K$, and assigning the second term as:

$$\delta_\xi^T \left( \delta_\eta + \dot{\delta}_\xi \right) \leq -K$$

Using the fact that $\dot{\delta}_\xi$ has system dynamics included in it, we can then determine a control policy to drive the error to zero. Using the system dynamics as defined in Section 4.2:

$$\begin{aligned} \delta_\eta + \dot{\delta}_\xi &\leq -K\delta_\xi \\ \dot{\xi} &\leq -K\delta_\xi - \delta_\eta + \dot{\xi}_r \\ F_b + G_b u &\leq -K\delta_\xi - \delta_\eta + \dot{\xi}_r \\ u &= -G_b^\dagger \left( K\delta_\xi + \delta_\eta - \dot{\xi}_r + F_b \right) \end{aligned}$$

In order to make the controller more effective, we can make $K$ a positive definite matrix, thus allowing us to have more adjustment over prioritizing the different states of the vehicle.

### *4.4 Controller Implementation*

In order to implement the backstepping control with error dynamics into our system, we first defined the $\eta$ and $\xi$ states:

$$\eta = \begin{bmatrix} \mathbf{b} \\ R \\ S \end{bmatrix} \qquad \xi = \begin{bmatrix} V_c \\ \Omega_c \\ \dot{S} \end{bmatrix}$$

We were then able to define the system dynamics in relation to the backstepping dynamics:

$$F_a = 0 \qquad G_a = \begin{bmatrix} R & 0 & 0 \\ 0 & R^{\wedge} & 0 \\ 0 & 0 & 1 \end{bmatrix}$$

$$F_b = \begin{bmatrix} g_0(R, S, V, \Omega, \dot{S}) \\ h_0(R, S, V, \Omega, \dot{S}) \\ 0 \end{bmatrix} \qquad G_{b_i} = \begin{bmatrix} g_i(S) \\ h_i(S) \\ e_i \end{bmatrix}$$

where $G_b = [G_{b_1}\ G_{b_2}\ G_{b_3}\ G_{b_4}]$, $e_i$ is a basis vector for the $i$th control, and $R^{\wedge}$ denotes a non-square matrix where $R^{\wedge}\Omega_c$ is equal to the vertically concatenated columns of $R\hat{\Omega}_c$.

In order to implement the control policy into our system, and only receive four control inputs, it was necessary to alter $G_b$ slightly. Whereas the equations of motion as describe in Section 2.3 utilize deflections $S_i \in \mathbb{R}^3$, due to physical constraints on the system, it is only actually possible to control wing deflection about the $y_i$ axis. For this reason, all terms corresponding to a $x_i$ or $z_i$ wing deflection were removed from $G_b$. We then find our system control policy to be:

$$u = -G_b^{\dagger}\left(K\delta_{\xi} + \delta_{\eta} - \dot{\xi}_r + F_b\right).$$

# Chapter 5
# SIMULATION RESULTS

In this section we will present the results of the system simulations of equilibria from the nonlinear study, both with and without angular perturbations from the initial conditions. We will then present results of the simulated system with control.

## *5.1 Uncontrolled Equilibria Simulation Results*

In order to first verify that the code was working properly, a series of uncontrolled, unperturbed simulations were run with the wings of the vehicle all deflected evenly at $0°, 45°$, and $90°$. These simulations were used to verify that the unperturbed system would fall straight down, and that as less surface area was exposed to the freestream air velocity, the terminal velocity of the system would increase to match theoretical values. An example of this verification can be found in Fig. 5.1.

Once the code was sufficiently verified, perturbations were introduced into the initial conditions of the system. For each of the cases below, the system was perturbed $10°$ about its $y_c$ axis.

### *5.1.1 No Spin, Effect of $V_2$*

The first simulation to examine is the system without spin and with an initial perturbation about the $y_c$ axis that will induce a velocity in the $x_c$ direction. We will examine two cases, one with the wings flat and another with the wings deflected at $45°$. In Fig. 5.2, we see the velocities of the vehicle in two cases: with $v_2$ (the velocity in the $y_c$ direction) initially at 0, and with $v_2$ initially at 0.1[m/s]. The resulting plots show that the effects of the perturbation on the $x_c$ velocity are independent of the initial value of $v_2$, and that the value

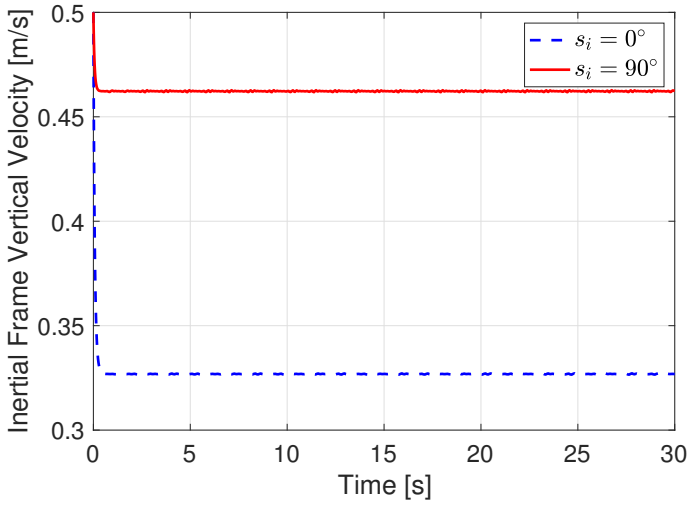


Figure 5.1: Vertical velocities of the unperturbed RoboRay, with wings flat and folded at 90°.

of $v_2$ is constant throughout.

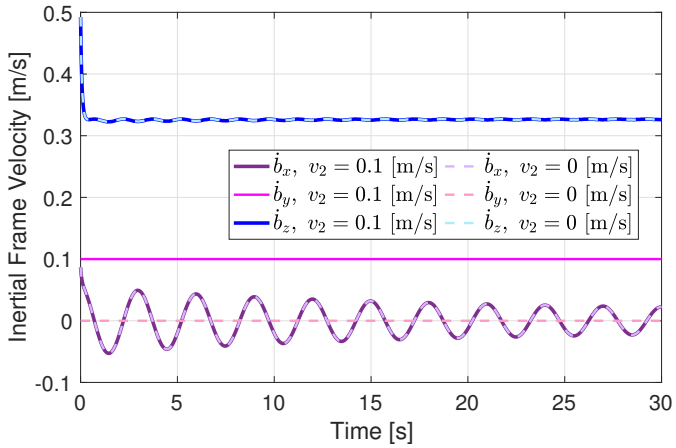


Figure 5.2: Velocities of the vehicle with an initial perturbation and $s_i = 0°$

In the second configuration with the same initial conditions, the wings are deflected at $s_i = 45°$; the plot of the velocities can be found in Fig. 5.3. In this case, we see that the vehicle with an initial velocity experiences more oscillations in its velocities throughout the

simulations. We also see that for the case where $v_2 = 0$, that initial zero component of the velocity is maintained throughout the simulation. This likely occurs as a result of the wing deflection coupled with the translational velocity having a differential moment on the even numbered wings. As the drag forces slow down the rotation, we see the moment difference happening in the reverse direction. This back and forth behavior is known as feathering, and is similar to the motion of a lightweight object such as a feather or leaf falling through the air.

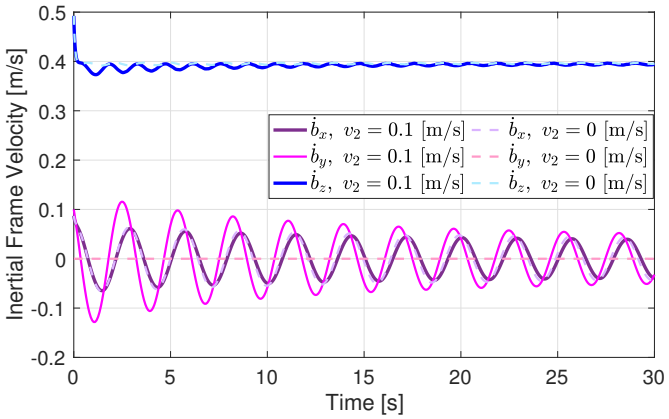


Figure 5.3: Velocities of the vehicle with an initial perturbation and $s_i = 45°$

### *5.1.2 Effect of Spin on Perturbations*

The next comparison of simulations will involve perturbing two systems, one with an initial spin about its $z_c$ axis, and one with no initial spin. In Fig. 5.4, we see that the perturbation creates a feathering effect in the $x_c$ direction, which in term creates some oscillations in the $z_c$ velocity. It does not appear to have any affect on the $y_c$ direction velocity.

Alternatively, we see in Fig. 5.5 that for the system with an initial rotational velocity in about the $z_c$ axis, there is an effect on the velocity in both the $x_c$ and $y_c$ velocity terms. The velocities in the two directions appear to be not only oscillating on their own, but also switching in magnitudes. This likely corresponds to a large, circular motion of the vehicle

with banked curves, similar to a multi-dimensional feathering.

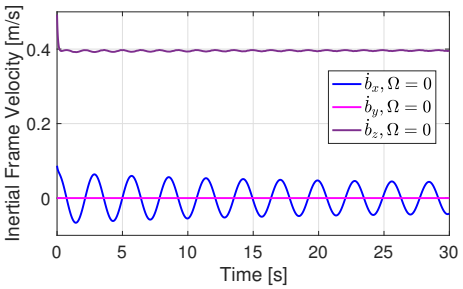


Figure 5.4: The effects of a perturbation on the translational velocities of a system with no spin and no initial horizontal velocity with $s_i = 45°$.

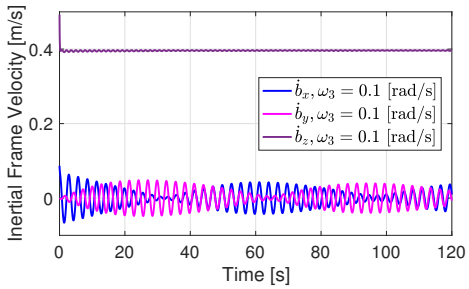


Figure 5.5: The effects of a perturbation on the translational velocities of a system with no initial horizontal velocity, but with an initial rotational velocity of $\Omega_3 = 0.1$ [rad/s] and $s_i = 45°$.

In examining the rotational velocities of the same two system simulations, we see similar effects. In Fig. 5.6 we see that the perturbation in the system without an initial rotational velocity causes a rotation about only one axis. For the rotational velocity of the system with spin, we see in Fig. 5.7 a behavior similar to the effects on the rotational velocities. Interestingly, though the initial rotational velocity clearly has an effect on the behavior of the system after the perturbation, the rotational velocity about the $z_c$ axis appears to remain unchanged.

### *5.1.3 Comparison of Effects of Initial Rotational and Translational Velocities on Perturbed System*

In this section, we will examine the performance of a system with an initial horizontal velocity term in comparison with a system with an initial rotational velocity term about its $z_c$ axis. In Figures 5.8 and 5.9, we see behavior similar to previous simulations. It is apparent in this case that the maximum magnitude of the oscillations in $\dot{b}_y$ of the simulation without spin are more than twice as large as the oscillations in the simulation with spin. Additionally, the simulation with spin seems to have its two velocity directions coupled, while there is

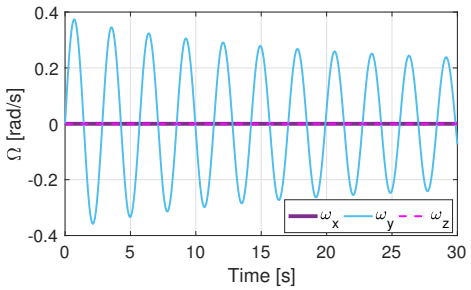


Figure 5.6: The effects of a perturbation on the rotational velocities of a system with no spin and no initial horizontal velocity with $s_i = 45°$.

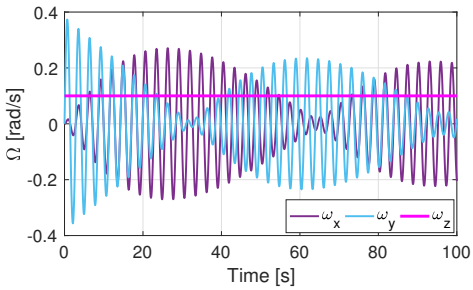


Figure 5.7: The effects of a perturbation on the rotational velocities of a system with no initial horizontal velocity, but with an initial rotational velocity of $\Omega_3 = 0.1$ [rad/s] and $s_i = 45°$.

no apparent relation for the case without spin. Finally, we seem in both cases that the maximum magnitude of the oscillations over time appears to be decreasing.

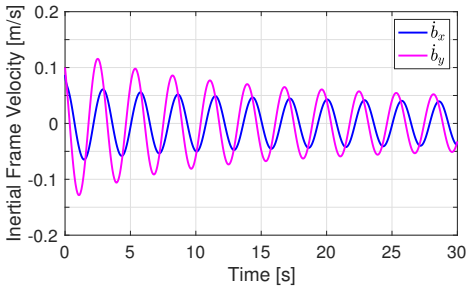


Figure 5.8: The effects of a perturbation on the translation velocities of a system with no spin, but with an initial horizontal velocity of $v_2 = 0.1$ [m/s] and $s_i = 45°$.

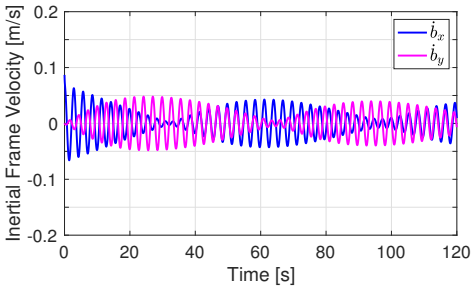


Figure 5.9: The effects of a perturbation on the translational velocities of a system with no initial horizontal velocity, but with an initial rotational velocity of $\Omega_3 = 0.1$ [rad/s] and $s_i = 45°$.

In Figures 5.10 and 5.11, we see similar results for the rotational velocities of the two systems. The simulation with no initial spin has larger magnitudes and no apparent coupling between the two directions of the rotational velocity. The simulation with the initial spin has smaller magnitudes overall, and apparent coupling. In both cases, again, we see a decay

in the maximum magnitude of the oscillations.

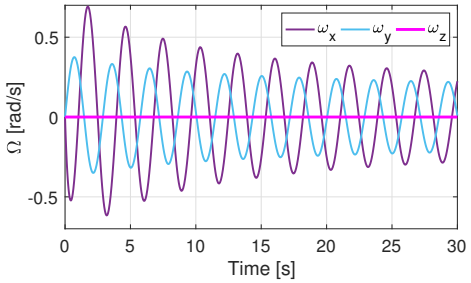


Figure 5.10: The effects of a perturbation on the translation velocities of a system with no spin, but with an initial horizontal velocity of $v_2 = 0.1$ [m/s] and $s_i = 45°$.

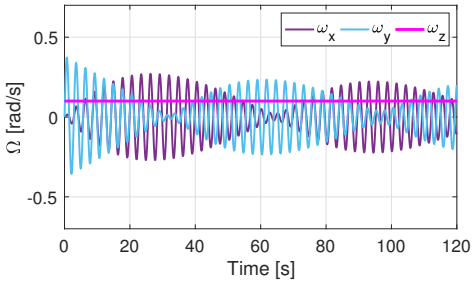


Figure 5.11: The effects of a perturbation on the translational velocities of a system with no initial horizontal velocity, but with an initial rotational velocity of $\Omega_3 = 0.1$ [rad/s] and $s_i = 45°$.

## *5.2 Controlled Simulation Results*

In this section we present the results from two different simulations implementing control. In the first simulation, we do a direct comparison between a simulation without control and a simulation with the same initial conditions, but now asking it to track a specified trajectory. In the second controlled simulation, we relax all of the constraints on the control, and simply ask it to implement a horizontal velocity.

### *5.2.1 Direct Comparison of Adding Control*

Figure 5.12 contains plots of the horizontal velocity components for the two simulations, controlled, and uncontrolled. Both simulations began with a rotational velocity about the $z_c$ axis of 0.5 [rad/s] and a translational velocity in the vertical direction of 0.3 [m/s]. The also began the simulations without perturbation, and with all of the wings folded up 45°. The controlled simulation was asked to track a trajectory in the positive $y_c$ direction at 0.3[m/s].

It is evident from the velocity plot that the controller did not have enough authority in order to maneuver the vehicle appropriately in the 60 seconds of simulation. While there

does seem to be a generally positive trend in the simulation, the total magnitude of the change is less than a millimeter, and thus effectively meaningless. An examination of Fig. 5.13 displays a slight change in the deflection of the wings, however it again suggests that there was not enough authority to properly maneuver.

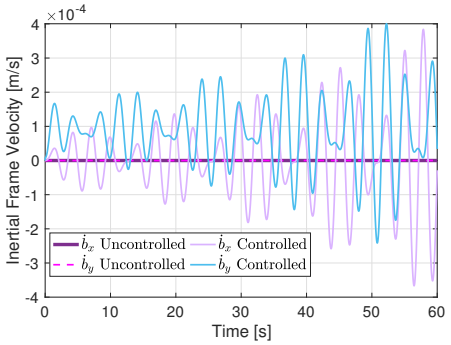


Figure 5.12: Translational velocities of the uncontrolled and controlled simulations with identical initial conditions.

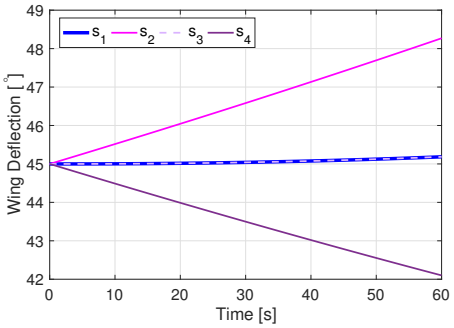


Figure 5.13: Wing deflections of the controlled simulation.

### *5.2.2 Relaxed Control Policy*

In this simulation, we start the vehicle with the same translational velocity as the previous, but now eliminate the rotational velocity. We also additionally weight the $K$ matrix of control more strongly towards tracking $y_c$ velocity. In Fig. 5.14 we see the vehicle moving in the $y_c$ direction, however it is actually moving in the incorrect direction. The increasing amplitude of the oscillations also suggest that it may be starting to experience some instability, though a longer simulation time would be required to say with any certain. The plot of the wing deflections in Fig. 5.15 shows that the wings appear to be returning toward their original state, suggesting that the vehicle may be trying to regain stability.

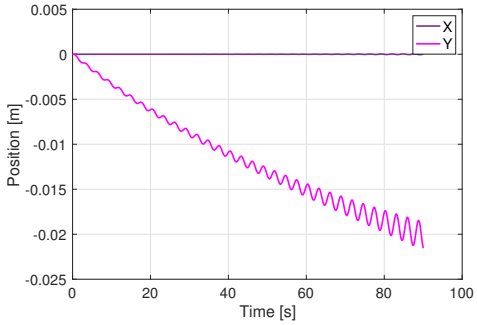


Figure 5.14: The horizontal positions versus time of the second control simulation.

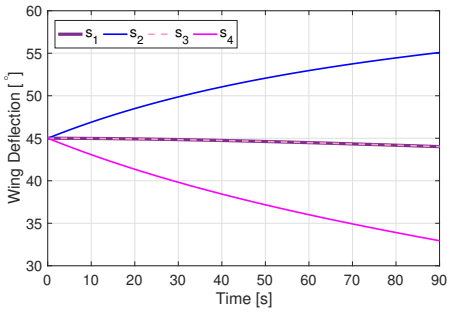


Figure 5.15: The wing deflections of the second control simulation.

### *5.3 Discussion of results*

In the uncontrolled simulations, we generally saw better overall performance in the systems with an initial spin about the $z_c$ axis. In the systems with an initial horizontal component of the velocity, we were more likely to see feathering in a single direction. On the other hand, in systems with an initial spin component, a behavior that appears to correspond to a 2-dimensional feathering occurs.

In the controlled system simulations, when the controller was tuned to weight the horizontal velocity more heavily, it seemed to have more control authority to deflect the wings appropriately and be able to track horizontally. Unfortunately, it did so in the wrong direction, and it isn't possible to understand how the system behavior would evolve without a longer time horizon. It is also possible that the initial rotational velocity in the first simulation resulted in the system having a strong enough equilibrium that the control was unable to force the system to leave.

# Chapter 6

# CONCLUSIONS

In this work we began developing the framework for model and control development for small, lightweight robotic systems designed for descent through fluids. We created a model of the system, complete with fluid dynamics considerations and equations of motion. We then found system equilibria and bounds for stability of those equilibria. Finally, we developed a controller to track a trajectory, and performed simulations of both the controlled and uncontrolled system.

The system simulations provided some potential insight into the behavior we can expect to see. First, the system is likely to experience feathering as it descends, whether that is in one or two dimensions. It is also likely that if the system enters a flat-spin, it will have difficultly leaving that equilibrium. Finally, we found that in order to properly control the vehicle, a great deal of tuning would need to be done, and it is likely that experimental analysis of the physical system will be necessary.

## *6.1 Future Work*

As this project is currently in its very early stages, we intend to continue developing both the model and the physical robot over the coming months and years. Early priorities will include continuing to tune the backstepping controller for improved performance and utilizing higher performance computing systems to reduce machine and round off errors that may be present. The physical robot is scheduled to be completed in Winter 2019, at which time the simulation results will be compared with experimental data in order to determine the accuracy of the model.

We also plan to implement a higher fidelity fluid dynamics model, in order to better

predict the behavior of the system. The improved model will be used in the development of the control for the space and reentry vehicles of similar design. As we move to the next iteration of the design, we intend to implement soft actuation in order to create a smooth, flexible vehicle.

# BIBLIOGRAPHY

[1] Justin A Atchison and Mason A Peck. A passive, sun-pointing, millimeter-scale solar sail. *Acta Astronautica*, 67(1-2):108–121, 2010.

[2] NASA Glenn Research Center. Shape effects on drag. `https://www.grc.nasa.gov/www/k-12/airplane/shaped.html`. Accessed: 2018-09-15.

[3] Rodolfo WL Coutinho, Azzedine Boukerche, Luiz FM Vieira, and Antonio AF Loureiro. Geographic and opportunistic routing for underwater sensor networks. *IEEE Transactions on Computers*, 65(2):548–561, 2016.

[4] Joshua Grady Graver. *Underwater gliders: Dynamics, control and design*. PhD thesis, Citeseer, 2005.

[5] Hassan K Khalil. *Nonlinear control*. Pearson New York, 2015.

[6] Sir Horace Lamb. *Hydrodynamics*. Cambridge University Press, 6th edition, 1932.

[7] Keum W Lee and Sahjendra N Singh. Nonlinear adaptive trajectory control of multi-input multi-output submarines with input constraints. *Proceedings of the Institution of Mechanical Engineers, Part I: Journal of Systems and Control Engineering*, 230(2):164–183, 2016.

[8] Uichin Lee, Paul Wang, Youngtae Noh, Luiz FM Vieira, Mario Gerla, and Jun-Hong Cui. Pressure routing for underwater sensor networks. In *INFOCOM, 2010 Proceedings IEEE*, pages 1–9. IEEE, 2010.

[9] Naomi Ehrich Leonard. Stability of a bottom-heavy underwater vehicle. *Automatica*, 33(3):331–346, 1997.

[10] Naomi Ehrich Leonard and Joshua G Graver. Model-based feedback control of autonomous underwater gliders. *IEEE Journal of oceanic engineering*, 26(4):633–645, 2001.

[11] Frank S Malvestuto and Lawrence J Gale. Formulas for additional mass corrections to the moments of inertia of airplanes. 1947.

[12] Zachary Manchester. Centimeter-scale spacecraft: Design, fabrication, and deployment. 2015.

[13] Zachary Manchester, Mason Peck, and Andrew Filo. Kicksat: A crowd-funded mission to demonstrate the worlds smallest spacecraft. 2013.

[14] Kristi A. Morgansen. Lecture notes on nonlinear control, June 2012.

[15] Kristi A Morgansen, Benjamin I Triplett, and Daniel J Klein. Geometric methods for modeling and control of free-swimming fin-actuated underwater vehicles. *IEEE Transactions on Robotics*, 23(6):1184–1199, 2007.

[16] Zexiang Li Richard M. Murray and S. Shankar Sastry. *A Mathematical Introduction to Robotic Manipulators*. CRC Press LLC, 1994.

[17] Peter Ridley, Julien Fontan, and Peter Corke. Submarine dynamic modelling. In *Proceedings of the 2003 Australasian Conference on Robotics & Automation*. Australian Robotics & Automation Association, 2003.

[18] David A Smallwood and Louis L Whitcomb. Model-based dynamic positioning of underwater robotic vehicles: theory and experiment. *IEEE Journal of Oceanic Engineering*, 29(1):169–186, 2004.

[19] Sisi Wang, Lijun Wang, Zixuan Qiao, and Fengshan Li. Optimal robust control of path following and rudder roll reduction for a container ship in heavy waves. *Applied Sciences*, 8(9):1631, 2018.

[20] Martin Wermuth, Gabriella Gaias, and Simone DAmico. Safe picosatellite release from a small satellite carrier. *Journal of Spacecraft and Rockets*, 52(5):1338–1347, 2015.

[21] E Jay Wyatt, Konstantin Belov, Julie Castillo-Rogez, Steve Chien, Abigail Fraeman, Jay Gao, Sebastian Herzig, et al. Autonomous networking for robotic deep space exploration. 2018.

[22] Wenjing Xie, Baoli Ma, Tyrone Fernando, and Herbert Ho-Ching Iu. A simple robust control for global asymptotic position stabilization of underactuated surface vessels. *International Journal of Robust and Nonlinear Control*, 27(18):5028–5043, 2017.

# Appendix A

# DEVELOPMENT OF THE EQUATIONS OF MOTION

The development of the equations of motion follows Lagrangian dynamics. The required steps are detailed here. First, we need to be able to express the different components in terms of the central vehicle frame.

$$
\begin{aligned}
M_i &= R_i M_{w_i} R_i^T \\
J_i &= R_i J_{w_i} R_i^T \\
V_i &= V_c - \hat{r}_{LE_i}\Omega_c - R_i \hat{r}_{CG_i}\dot{S}_i \\
\Omega_i &= \Omega_c + R_i \dot{S}_i
\end{aligned}
$$

$$
\begin{aligned}
V_i^T M_i V_i &= \left(V_c^T + \Omega_c^T \hat{r}_{LE_i} + \dot{S}_i^T \hat{r}_{CG_i} R_i^T\right) M_i \left(V_c - \hat{r}_{LE_i}\Omega_c - R_i \hat{r}_{CG_i}\dot{S}_i\right) \\
&= V_c^T M_i V_c - V_c^T M_i \hat{r}_{LE_i}\Omega_c - V_c^T M_i R_i \hat{r}_{CG_i}\dot{S}_i + \Omega_c^T \hat{r}_{LE_i} M_i V_c \\
&\quad - \Omega_c^T \hat{r}_{LE_i} M_i \hat{r}_{LE_i}\Omega_c - \Omega_c^T \hat{r}_{LE_i} M_i R_i \hat{r}_{CG_i}\dot{S}_i \\
&\quad + \dot{S}_i^T \hat{r}_{CG_i} R_i^T M_i V_c - \dot{S}_i^T \hat{r}_{CG_i} R_i^T M_i \hat{r}_{LE_i}\Omega_c - \dot{S}_i^T \hat{r}_{CG_i} M_{w_i} \hat{r}_{CG_i}\dot{S}_i
\end{aligned}
$$

$$
\begin{aligned}
\Omega_i^T J_i \Omega_i &= \left(\Omega_c^T + \dot{S}_i^T R_i^T\right) J_i \left(\Omega_c + R_i \dot{S}_i\right) \\
&= \Omega_c^T J_i \Omega_c + \Omega_c^T J_i R_i \dot{S}_i + \dot{S}_i^T R_i^T J_i \Omega_c + \dot{S}_i^T J_{w_i} \dot{S}_i
\end{aligned}
$$

This allows us to define the following system matrices, and our Lagrangian:

$$\tilde{M} = M_c + \sum_{i=1}^{4} M_i$$

$$\tilde{D} = D_c + \sum_{i=1}^{4} \hat{r}_{LE_i} M_i$$

$$\tilde{J} = J_c + \sum_{i=1}^{4} J_i - \hat{r}_{LE_i} M_i \hat{r}_{LE_i}$$

$$L = \frac{1}{2} \begin{bmatrix} V_c \\ \Omega_c \\ \dot{S} \end{bmatrix}^T \begin{bmatrix} \tilde{M} & \tilde{D}^T & \mathcal{A}_1^T \\ \tilde{D} & \tilde{J} & \mathcal{A}_2^T \\ \mathcal{A}_1 & \mathcal{A}_2 & \mathcal{I} \end{bmatrix} \begin{bmatrix} V_c \\ \Omega_c \\ \dot{S} \end{bmatrix} - U$$

Where the matrices in our Lagrangian Dynamics are:

$$\mathcal{A} = \begin{bmatrix} \hat{r}_{CG_1} M_{w_1} R_1^T & -\hat{r}_{CG_1} M_{w_1} R_1^T \hat{r}_{LE_1} \\ \hat{r}_{CG_2} M_{w_2} R_2^T & -\hat{r}_{CG_2} M_{w_2} R_2^T \hat{r}_{LE_2} \\ \hat{r}_{CG_3} M_{w_3} R_3^T & -\hat{r}_{CG_1} M_{w_3} R_3^T \hat{r}_{LE_3} \\ \hat{r}_{CG_4} M_{w_4} R_4^T & -\hat{r}_{CG_4} M_{w_4} R_4^T \hat{r}_{LE_4} \end{bmatrix}$$

$$\mathcal{I} = \text{Diag}\Big( J_{w_1} - \hat{r}_{CG_1} M_{w_1} r_{CG_1},\ J_{w_2} - \hat{r}_{CG_2} M_{w_2} r_{CG_2},$$

$$J_{w_3} - \hat{r}_{CG_3} M_{w_3} r_{CG_3},\ J_{w_4} - \hat{r}_{CG_4} M_{w_4} r_{CG_4} \Big)$$

And our potential energy term is:

$$U = -m_v a_w l(R^T \mathbf{k} \cdot \mathbf{z}_c) + m_v a_w (\mathbf{b} \cdot \mathbf{k})$$

Using Lagrange's equations we can take partial derivatives of the system to determine the equations of motion:

$$
\begin{aligned}
\frac{\partial L}{\partial V_c} &= V_c^T \tilde{M} + \dot{S}^T \mathcal{A}_1 + \Omega_c^T \tilde{D} \\
\frac{\partial L}{\partial b} &= m_v a_w \mathbf{k} \\
\frac{\partial L}{\partial \Omega_c} &= V_c^T \tilde{D}^T + \Omega_c^T \tilde{J} + \dot{S}^T \mathcal{A}_2 \\
\frac{\partial L}{\partial R} &= -m_v a_w l (R^T \mathbf{k} \times \mathbf{z}_c) \\
\frac{\partial L}{\partial \dot{S}} &= V_c^T \mathcal{A}_1^T + \Omega_c^T \mathcal{A}_2^T + \dot{S}^T \mathcal{I} \\
\frac{\partial L}{\partial S} &= \frac{1}{2} V_c^T \frac{\partial}{\partial S} \left( \tilde{M} \right) V_c + \Omega_c^T \frac{\partial}{\partial S} \left( \tilde{D} \right) V_c + \frac{1}{2} \Omega_c^T \frac{\partial}{\partial S} \left( \tilde{J} \right) \Omega_c \\
&\quad + V_c^T \frac{\partial}{\partial S} \left( \mathcal{A}_1^T \right) \dot{S} + \Omega_c^T \frac{\partial}{\partial S} \left( \mathcal{A}_2^T \right) \dot{S}
\end{aligned}
$$

$$
\begin{aligned}
\frac{d}{dt} \left( \frac{\partial L}{\partial V_c} \right) &= \dot{V}_c^T \tilde{M} + V_c^T \dot{\tilde{M}} + \ddot{S}^T \mathcal{A}_1 + \dot{S}^T \dot{\mathcal{A}}_1 + \dot{\Omega_c}^T \tilde{D} + \Omega_c^T \dot{\tilde{D}} \\
\frac{d}{dt} \left( \frac{\partial L}{\partial \Omega_c} \right) &= \dot{V}_c^T \tilde{D}^T + V_c^T \dot{\tilde{D}}^T + \dot{\Omega}_c^T \tilde{J} + \Omega_c^T \dot{\tilde{J}} + \ddot{S}^T \mathcal{A}_2 + \dot{S}^T \dot{\mathcal{A}}_2 \\
\frac{d}{dt} \left( \frac{\partial L}{\partial \dot{S}} \right) &= \dot{V}_c^T \mathcal{A}_1^T + V_c^T \dot{\mathcal{A}}_1^T + \dot{\Omega}_c^T \mathcal{A}_2^T + \Omega_c^T \dot{\mathcal{A}}_2^T + \ddot{S}^T \mathcal{I} + \dot{S}^T \dot{\mathcal{I}}
\end{aligned}
$$

Algebraic Solving for the second derivative terms provides:

$$
\begin{aligned}
\dot{V}_c \;&= m_v a_w C \mathbf{k} - m_v a_w \ell B (R^T \mathbf{k} \times z_c) + C F_{ext} + B M_{ext} - \left( C \dot{\tilde{M}} + B \dot{\tilde{D}} \right) V_c \\
&\quad - \left( C \dot{\tilde{D}}^T + B \dot{\tilde{J}} \right) \Omega_c - \left( C \dot{\mathcal{A}}_1^T + B \dot{\mathcal{A}}_2^T \right) \dot{S} - \left( C \mathcal{A}_1^T + B \mathcal{A}_2^T \right) \ddot{S}
\end{aligned} \tag{A.1}
$$

$$
\begin{aligned}
\dot{\Omega}_c \;&= m_v a_w B^T \mathbf{k} - m_v a_w \ell A (R^T \mathbf{k} \times z_c) + B^T F_{ext} + A M_{ext} - \left( B^T \dot{\tilde{M}} + A \dot{\tilde{D}} \right) V_c \\
&\quad - \left( B^T \dot{\tilde{D}}^T + A \dot{\tilde{J}} \right) \Omega_c - \left( B^T \dot{\mathcal{A}}_1^T + A \dot{\mathcal{A}}_2^T \right) \dot{S} - \left( B^T \mathcal{A}_1^T + A \mathcal{A}_2^T \right) \ddot{S}
\end{aligned} \tag{A.2}
$$

$$
\ddot{S} \;= u \tag{A.3}
$$

# Appendix B

# NONLINEAR STABILITY ANALYSIS

$$\breve{J} = \begin{bmatrix} I_1 & 0 & 0 \\ 0 & I_2 & 0 \\ 0 & 0 & I_3 \end{bmatrix}$$

$$\breve{M} = \begin{bmatrix} m_1 & 0 & 0 \\ 0 & m_2 & 0 \\ 0 & 0 & m_3 \end{bmatrix}$$

$$\breve{D} = \begin{bmatrix} 0 & -d_1 & 0 \\ d_2 & 0 & 0 \\ 0 & 0 & 0 \end{bmatrix}$$

## *B.1 No Spin Equilibrium:*

$$\Omega_{e1} = \begin{bmatrix} 0 \\ 0 \\ 0 \end{bmatrix} \quad V_{e1} = \begin{bmatrix} 0 \\ v_{e1_2} \\ v_{e1_3} \end{bmatrix} \quad \Gamma_{e1} = \begin{bmatrix} 0 \\ \frac{(m_2-m_3)v_{e1_2}v_{e1_3}}{m_v a_w \ell} \\ \sqrt{1-\left(\frac{(m_2-m_3)v_{e1_2}v_{e1_3}}{m_v a_w \ell}\right)^2} \end{bmatrix}$$

$$\Pi_e = \breve{D}V_{e1} = \begin{bmatrix} -d_1 v_{e1_2} \\ 0 \\ 0 \end{bmatrix} \qquad P_e = \breve{M}V_{e1} = \begin{bmatrix} 0 \\ m_2 v_{e1_2} \\ m_3 v_{e1_3} \end{bmatrix}$$

$$H = \frac{1}{2}\left(\Pi^T \breve{A}\Pi + 2\Pi^T \breve{B}^T P + P^T \breve{C} P\right) - m_v a_w \ell(\Gamma \cdot z_c)$$

$$H_\Phi = H + \Phi(P \cdot \Gamma, \|P\|^2, \|\Gamma\|^2)$$

$$\nabla H = \begin{bmatrix} \breve{A}\Pi + \breve{B}^T P \\ \breve{B}\Pi + \breve{C} P \\ -m_v a_w \ell z_c \end{bmatrix} = \begin{bmatrix} 0 \\ 0 \\ 0 \\ 0 \\ v_{e1_2} \\ v_{e1_3} \\ 0 \\ 0 \\ -m_v a_w \ell \end{bmatrix}$$

$$\nabla\Phi(P\cdot\Gamma, \|P\|^2, \|\Gamma\|^2) = \begin{bmatrix} \frac{\partial\Phi}{\partial\Pi} \\ \frac{\partial\Phi}{\partial P} \\ \frac{\partial\Phi}{\partial\Gamma} \end{bmatrix} = \begin{bmatrix} \frac{\partial\Phi}{\partial C_1}\frac{\partial C_1}{\partial\Pi} + \frac{\partial\Phi}{\partial C_2}\frac{\partial C_2}{\partial\Pi} + \frac{\partial\Phi}{\partial C_3}\frac{\partial C_3}{\partial\Pi} \\ \frac{\partial\Phi}{\partial C_1}\frac{\partial C_1}{\partial P} + \frac{\partial\Phi}{\partial C_2}\frac{\partial C_2}{\partial P} + \frac{\partial\Phi}{\partial C_3}\frac{\partial C_3}{\partial P} \\ \frac{\partial\Phi}{\partial C_1}\frac{\partial C_1}{\partial\Gamma} + \frac{\partial\Phi}{\partial C_2}\frac{\partial C_2}{\partial\Gamma} + \frac{\partial\Phi}{\partial C_3}\frac{\partial C_3}{\partial\Gamma} \end{bmatrix}$$

$$= \begin{bmatrix} 0 \\ \dot{\Phi}\Gamma_e + 2\Phi' P_e \\ \dot{\Phi} P_e + 2\Phi^\dagger \Gamma_e \end{bmatrix}$$

$$\begin{bmatrix} 0 \\ 0 \\ 0 \\ 0 \\ v_{e1_2} \\ v_{e1_3} \\ 0 \\ 0 \\ -m_v a_w \ell \end{bmatrix} = - \begin{bmatrix} 0 \\ 0 \\ 0 \\ 0 \\ \dot{\Phi}\frac{(m_2-m_3)v_{e1_2}v_{e1_3}}{m_v a_w \ell} + 2\Phi' m_2 v_{e1_2} \\ \dot{\Phi}\sqrt{1-\left(\frac{(m_2-m_3)v_{e1_2}v_{e1_3}}{m_v a_w \ell}\right)^2} + 2\Phi' m_3 v_{e1_3} \\ 0 \\ \dot{\Phi} m_2 v_{e1_2} + 2\Phi^\dagger \frac{(m_2-m_3)v_{e1_2}v_{e1_3}}{m_v a_w \ell} \\ \dot{\Phi} m_3 v_{e1_3} + 2\Phi^\dagger \sqrt{1-\left(\frac{(m_2-m_3)v_{e1_2}v_{e1_3}}{m_v a_w \ell}\right)^2} \end{bmatrix}$$

If $\dot{\Phi} = 0$ and $v_{e1_2} = 0$:

$$\begin{bmatrix} 0 \\ 0 \\ 0 \\ 0 \\ 0 \\ v_{e1_3} \\ 0 \\ 0 \\ -m_v a_w \ell \end{bmatrix} = - \begin{bmatrix} 0 \\ 0 \\ 0 \\ 0 \\ 0 \\ 2\Phi' m_3 v_{e1_3} \\ 0 \\ 0 \\ 2\Phi^\dagger \end{bmatrix}$$

$$2\Phi' = -1/(m_3)$$

$$2\Phi^\dagger = m_v a_w \ell$$

$$\nabla^2 H = \begin{bmatrix} \breve{A} & \breve{B}^T & 0 \\ \breve{B} & \breve{C} & 0 \\ 0 & 0 & 0 \end{bmatrix}$$

$$\nabla^2 \Phi(P \cdot \Gamma, \|P\|^2, \|\Gamma\|^2) = \begin{bmatrix} 0 & 0 & 0 \\ 0 & \frac{\partial}{\partial P}\left(\dot{\Phi}\Gamma_e + 2\Phi' P_e\right) & \frac{\partial}{\partial \Gamma}\left(\dot{\Phi}\Gamma_e + 2\Phi' P_e\right) \\ 0 & \frac{\partial}{\partial P}\left(\dot{\Phi} P_e + 2\Phi^\dagger \Gamma_e\right) & \frac{\partial}{\partial \Gamma}\left(\dot{\Phi} P_e + 2\Phi^\dagger \Gamma_e\right) \end{bmatrix}$$

$$\frac{\partial}{\partial P}\left(\dot{\Phi}\Gamma_e + 2\Phi' P_e\right) = \ddot{\Phi}\Gamma_e \Gamma_e^T + 2\dot{\Phi}'\Gamma_e P_e^T + 2\left(\dot{\Phi}' P_e \Gamma_e^T + 2\Phi'' P_e P_e^T + \Phi' I\right)$$

$$\frac{\partial}{\partial \Gamma}\left(\dot{\Phi}\Gamma_e + 2\Phi' P_e\right) = \ddot{\Phi}\Gamma_e P_e^T + 2\dot{\Phi}^\dagger \Gamma_e \Gamma_e^T + \dot{\Phi} I + 2\left(\dot{\Phi}' P_e P_e^T + 2\Phi^{\dagger\prime} P_e \Gamma_e^T\right)$$

$$\frac{\partial}{\partial P}\left(\dot{\Phi} P_e + 2\Phi^\dagger \Gamma_e\right) = \ddot{\Phi} P_e \Gamma_e^T + 2\dot{\Phi}' P_e P_e^T + \dot{\Phi} I + 2\left(\dot{\Phi}^\dagger \Gamma_e \Gamma_e^T + 2\Phi^{\dagger\prime} \Gamma_e P_e^T\right)$$

$$\frac{\partial}{\partial \Gamma}\left(\dot{\Phi} P_e + 2\Phi^\dagger \Gamma_e\right) = \ddot{\Phi} P_e P_e^T + 2\dot{\Phi}^\dagger P_e \Gamma_e^T + 2\left(\dot{\Phi}^\dagger \Gamma_e P_e^T + 2\Phi^{\dagger\dagger} \Gamma_e \Gamma_e^T + \Phi^\dagger I\right)$$

$$a = \ddot{\Phi} \qquad b = 2\dot{\Phi}' \qquad c = 4\Phi''$$
$$d = 2\dot{\Phi}^{\dagger} \qquad e = 4\Phi^{\dagger\prime} \qquad f = 4\Phi^{\dagger\dagger}$$

Assuming $b = d = e = f = 0$

$$\frac{\partial}{\partial P}\left(\dot{\Phi}\Gamma_e + 2\Phi' P_e\right) = a\Gamma_e\Gamma_e^T + cP_eP_e^T - 1/m_3 I$$
$$\frac{\partial}{\partial \Gamma}\left(\dot{\Phi}\Gamma_e + 2\Phi' P_e\right) = a\Gamma_e P_e^T$$
$$\frac{\partial}{\partial P}\left(\dot{\Phi}P_e + 2\Phi^{\dagger}\Gamma_e\right) = aP_e\Gamma_e^T$$
$$\frac{\partial}{\partial \Gamma}\left(\dot{\Phi}P_e + 2\Phi^{\dagger}\Gamma_e\right) = aP_eP_e^T + m_v a_w \ell I$$

$$\Gamma_e\Gamma_e^T = \begin{bmatrix} 0 & 0 & 0 \\ 0 & 0 & 0 \\ 0 & 0 & 1 \end{bmatrix} \qquad P_eP_e^T = \begin{bmatrix} 0 & 0 & 0 \\ 0 & 0 & 0 \\ 0 & 0 & m_3^2 v_{e1_3}^2 \end{bmatrix}$$

$$\Gamma_e P_e^T = \begin{bmatrix} 0 & 0 & 0 \\ 0 & 0 & 0 \\ 0 & 0 & m_3 v_{e1_3} \end{bmatrix} \qquad P_e\Gamma_e^T = \begin{bmatrix} 0 & 0 & 0 \\ 0 & 0 & 0 \\ 0 & 0 & m_3 v_{e1_3} \end{bmatrix}$$

$\nabla^2 H + \nabla^2 \Phi$

$$= \begin{bmatrix} a_1 & 0 & 0 & 0 & b_2 & 0 & 0 & 0 & 0 \\ 0 & a_2 & 0 & b_1 & 0 & 0 & 0 & 0 & 0 \\ 0 & 0 & a_3 & 0 & 0 & 0 & 0 & 0 & 0 \\ 0 & b_1 & 0 & c_1 - \frac{1}{m_3} & 0 & 0 & 0 & 0 & 0 \\ b_2 & 0 & 0 & 0 & c_2 - \frac{1}{m_3} & 0 & 0 & 0 & 0 \\ 0 & 0 & 0 & 0 & 0 & c_3 + a + cm_3^2 v_{e1_3}^2 - \frac{1}{m_3} & 0 & 0 & am_3 v_{e1_3} \\ 0 & 0 & 0 & 0 & 0 & 0 & m_v a_w \ell & 0 & 0 \\ 0 & 0 & 0 & 0 & 0 & 0 & 0 & m_v a_w \ell & 0 \\ 0 & 0 & 0 & 0 & 0 & am_3 v_{e1_3} & 0 & 0 & m_v a_w \ell + am_3^2 v_{e1_3}^2 \end{bmatrix}$$

$LDL^T$ factorization

$$D_j = A_{jj} - \sum_{k=1}^{j-1} L_{jk}^2 D_k$$

$$L_{ij} = \frac{1}{D_j} \left( A_{ij} - \sum_{k=1}^{j-1} L_{ik} L_{jk} D_k \right) \qquad i > j$$

$$D_1 = a_1 \qquad D_2 = a_2 \qquad D_3 = a_3$$

$$D_4 = \frac{1}{m_1} - \frac{1}{m_3} \qquad D_5 = \frac{1}{m_2} - \frac{1}{m_3} \qquad D_6 = a + cm_3^2 v_{e1_3}^2$$

$$D_7 = m_v a_w \ell \qquad D_8 = m_v a_w \ell \qquad D_9 = m_v a_w \ell + \frac{acm_3^4 v_{e1_3}^4}{a + cm_3^2 v_{e1_3}^2}$$

$$L = \begin{bmatrix} 1 & 0 & 0 & 0 & 0 & 0 & 0 & 0 & 0 \\ 0 & 1 & 0 & 0 & 0 & 0 & 0 & 0 & 0 \\ 0 & 0 & 1 & 0 & 0 & 0 & 0 & 0 & 0 \\ 0 & -\frac{d_2}{m_1} & 0 & 1 & 0 & 0 & 0 & 0 & 0 \\ \frac{d_1}{m_2} & 0 & 0 & 0 & 1 & 0 & 0 & 0 & 0 \\ 0 & 0 & 0 & 0 & 0 & 1 & 0 & 0 & 0 \\ 0 & 0 & 0 & 0 & 0 & 0 & 1 & 0 & 0 \\ 0 & 0 & 0 & 0 & 0 & 0 & 0 & 1 & 0 \\ 0 & 0 & 0 & 0 & 0 & \frac{am_3 v_{e1_3}}{a+cm_3^2 v_{e1_3}^2} & 0 & 0 & 1 \end{bmatrix}$$

Sufficient Conditions for Stability:

- $\ell > 0$
- $m_3 > m_1$
- $m_3 > m_2$

### *B.2 Equilibrium with Spin*

$$\Omega_{e2} = \begin{bmatrix} 0 \\ 0 \\ \omega_{e2_3} \end{bmatrix} \quad V_{e2} = \begin{bmatrix} 0 \\ 0 \\ v_{e2_3} \end{bmatrix} \quad \Gamma_{e2} = \begin{bmatrix} 0 \\ 0 \\ 1 \end{bmatrix}$$

$$\Pi_e = \breve{J}\Omega_{e2} + \breve{D}V_{e2} = \begin{bmatrix} 0 \\ 0 \\ I_3\omega_{e2_3} \end{bmatrix} \qquad P_e = \breve{M}V_{e2} + \breve{D}^T\Omega_{e2} = \begin{bmatrix} 0 \\ 0 \\ m_3 v_{e2_3} \end{bmatrix}$$

$$\nabla H = -\nabla\Phi - \nabla\phi$$

$$\begin{bmatrix} 0 \\ 0 \\ \omega_{e2_3} \\ 0 \\ 0 \\ v_{e1_3} \\ 0 \\ 0 \\ -m_v a_w \ell \end{bmatrix} = - \begin{bmatrix} 0 \\ 0 \\ 0 \\ 0 \\ 0 \\ \dot{\Phi} + 2\Phi' m_3 v_{e1_3} \\ 0 \\ 0 \\ \dot{\Phi} m_3 v_{e1_3} + 2\Phi^\dagger \end{bmatrix} - \begin{bmatrix} 0 \\ 0 \\ \dot{\phi} \\ 0 \\ 0 \\ 0 \\ 0 \\ 0 \\ 0 \end{bmatrix}$$

$$\dot{\Phi} = 0 \qquad\qquad 2\Phi' = -1/m_3$$

$$\dot{\phi} = -\omega_{e2_3} \qquad\qquad 2\Phi^\dagger = m_v a_w \ell$$

$$\nabla^2\phi = \begin{bmatrix} \ddot{\phi} & 0 & 0 \\ 0 & 0 & 0 \\ 0 & 0 & 0 \end{bmatrix}$$

$$\ddot{\phi} = g$$

$$\nabla^2 H + \nabla^2 \Phi + \nabla^2 \phi$$

$$= \begin{bmatrix} a_1 & 0 & 0 & 0 & b_2 & 0 & 0 & 0 & 0 \\ 0 & a_2 & 0 & b_1 & 0 & 0 & 0 & 0 & 0 \\ 0 & 0 & a_3+g & 0 & 0 & 0 & 0 & 0 & 0 \\ 0 & b_1 & 0 & c_1 - \frac{1}{m_3} & 0 & 0 & 0 & 0 & 0 \\ b_2 & 0 & 0 & 0 & c_2 - \frac{1}{m_3} & 0 & 0 & 0 & 0 \\ 0 & 0 & 0 & 0 & 0 & c_3 + a + cm_3^2 v_{e1_3}^2 - \frac{1}{m_3} & 0 & 0 & am_3 v_{e1_3} \\ 0 & 0 & 0 & 0 & 0 & 0 & m_v a_w \ell & 0 & 0 \\ 0 & 0 & 0 & 0 & 0 & 0 & 0 & m_v a_w \ell & 0 \\ 0 & 0 & 0 & 0 & 0 & am_3 v_{e1_3} & 0 & 0 & m_v a_w \ell + am_3^2 v_{e1_3}^2 \end{bmatrix}$$

$LDL^T$ factorization

$$D_j = A_{jj} - \sum_{k=1}^{j-1} L_{jk}^2 D_k$$

$$L_{ij} = \frac{1}{D_j}\left(A_{ij} - \sum_{k=1}^{j-1} L_{ik} L_{jk} D_k\right) \qquad i > j$$

$$D_1 = a_1 \qquad D_2 = a_2 \qquad D_3 = a_3 + g$$

$$D_4 = \frac{1}{m_1} - \frac{1}{m_3} \qquad D_5 = \frac{1}{m_2} - \frac{1}{m_3} \qquad D_6 = a + cm_3^2 v_{e1_3}^2$$

$$D_7 = m_v a_w \ell \qquad D_8 = m_v a_w \ell \qquad D_9 = m_v a_w \ell + \frac{acm_3^4 v_{e1_3}^4}{a + cm_3^2 v_{e1_3}^2}$$

$$L = \begin{bmatrix} 1 & 0 & 0 & 0 & 0 & 0 & 0 & 0 & 0 \\ 0 & 1 & 0 & 0 & 0 & 0 & 0 & 0 & 0 \\ 0 & 0 & 1 & 0 & 0 & 0 & 0 & 0 & 0 \\ 0 & -\frac{d_2}{m_1} & 0 & 1 & 0 & 0 & 0 & 0 & 0 \\ \frac{d_1}{m_2} & 0 & 0 & 0 & 1 & 0 & 0 & 0 & 0 \\ 0 & 0 & 0 & 0 & 0 & 1 & 0 & 0 & 0 \\ 0 & 0 & 0 & 0 & 0 & 0 & 1 & 0 & 0 \\ 0 & 0 & 0 & 0 & 0 & 0 & 0 & 1 & 0 \\ 0 & 0 & 0 & 0 & 0 & \frac{am_3v_{e1_3}}{a+cm_3^2v_{e1_3}^2} & 0 & 0 & 1 \end{bmatrix}$$

Sufficient Conditions for Stability:

- $\ell > 0$
- $m_3 > m_1$
- $m_3 > m_2$

If $m_2 = m_3$

$$D_1 = \frac{m_2}{I_1 m_2 - d_1^2} \qquad D_2 = \frac{m_1}{I_2 m_1 - d_2^2} \qquad D_3 = \frac{1}{I_3}$$
$$D_4 = \frac{1}{m_1} - \frac{1}{m_2} \qquad D_5 = cm_2^2 v_{e1_2}^2 \qquad D_6 = a$$
$$D_7 = m_v a_w \ell \qquad D_8 = m_v a_w \ell$$

$$D_9 = \frac{m_v^2 a_w^2 \ell^2 - m_2^2 m_3^2 v_{e1_2}^2 v_{e1_3}^2 (1-a)^2}{m_v a_w \ell}$$

Conditions for stability:

- $a, c > 0$

- $m_2 > m_1$
- $m_v^2 a_w^2 \ell^2 > m_2^2 m_3^2 v_{e1_2}^2 v_{e1_3}^2 (1-a)^2$